NATIONAL ADVISORY COMMITTEE FOR AERONAUTICS

TECHNICAL NOTE 3285

SECTION CHARACTERISTICS OF AN NACA 0006 AIRFOIL WITH AREA SUCTION NEAR THE LEADING EDGE

By James A. Weiberg and Robert E. Dannenberg

Ames Aeronautical Laboratory
Moffett Field, Calif.

Washington

September 1954

NATIONAL ADVISORY COMMITTEE FOR AERONAUTICS

TECHNICAL NOTE 3285

SECTION CHARACTERISTICS OF AN NACA 0006 AIRFOIL WITH AREA SUCTION NEAR THE LEADING EDGE

By James A. Weiberg and Robert E. Dannenberg

SUMMARY

An investigation has been made of the low-speed two-dimensional aerodynamic characteristics of an NACA 0006 airfoil with area suction near the leading edge. The maximum lift coefficient of the airfoil was increased from 0.87 to 1.25 for a section flow coefficient of 0.0010 at a free-stream velocity of 162 feet per second.

From an analysis of the data presented in this report and in NACA TN 3093 (area suction on a 10.51-percent-thick airfoil), it was found that for a given increase in lift coefficient the minimum suction quantity required was related to the magnitude of the difference between the external pressure coefficients at the leading and trailing edges of the porous area.

INTRODUCTION

The maximum lift of symmetrical airfoils with thickness-chord ratios less than about 0.12 is generally limited by separation of the laminar boundary layer from the upper surface. The manner in which an airfoil stalls, however, is influenced by the thickness ratio and by the localized "bubble" of separated flow near the leading edge (ref. 1). Generally, for airfoils with a thickness-chord ratio of 0.06, the stall is classified as thin-airfoil stall and is preceded by flow separation near the leading edge with reattachment at a point which moves progressively downstream with increasing angle of attack. The stall occurs as the reattachment point coincides with the trailing edge. With increased thickness (to the order of 0.10), the flow separation preceding the stall is localized near the leading edge. At the stall, which is classified as a leading-edge stall, the flow separates abruptly from the leading edge without subsequent reattachment.

It has been demonstrated that suction through a porous area near the leading edge can eliminate the latter type of stall, with a resultant increase in the maximum lift (refs. 2 to 4). With adequate suction, the maximum lift of moderately thick airfoils (10 to 12 percent thick) is generally limited by the separation of the turbulent boundary layer

starting near the trailing edge. The effectiveness of leading-edge area suction in increasing the maximum lift of a 6-percent-thick airfoil has been open to some question, however, because of the different type of stall (i.e., thin-airfoil stall).

The experimental investigation reported herein was undertaken to ascertain the effectiveness of boundary-layer control on a thin two-dimensional airfoil - an NACA 0006. The model was equipped for area suction near the leading edge and with a 0.20-chord split flap. The tests were made in one of the Ames 7- by 10-foot wind tunnels and included measurements of the surface pressure distributions, lift, profile drag, suction requirements, and boundary-layer characteristics.

NOTATION

c airfoil chord, ft

c_{d_o} section profile-drag coefficient, $\frac{D}{q_o c}$, as determined from wake surveys

c_l section lift coefficient, $\frac{L}{q_o c}$

c_m section pitching-moment coefficient referred to the quarter-chord point, $\frac{M}{q_o c^2}$

c_Q section flow coefficient, $\frac{\int v \, ds}{c \, V_o}$
(The limits of integration are the foremost and rearmost points of area suction.)

c_w suction power coefficient (ref. 3),

$$\frac{1}{c q_o V_o} \left(\frac{\gamma}{\gamma-1}\right) Q_1 p_1 \left[\left(\frac{p_o}{p_1}\right)^{\frac{\gamma-1}{\gamma}} - 1\right]$$

D drag per unit span, lb

H boundary-layer shape parameter, $\frac{\delta^*}{\theta}$

Δh pressure difference across porous material, in. H_2O

L lift per unit span, lb

M pitching moment per unit span, referred to the quarter-chord point, lb-ft

P pressure coefficient, $\frac{p-p_o}{q_o}$

p static pressure, lb/sq ft

Q volume rate of flow per unit span, cu ft/sec

q_o free-stream dynamic pressure, $\frac{1}{2}\rho_o V_o^2$, lb/sq ft

s distance along airfoil surface, ft

t maximum airfoil thickness, ft

U local velocity outside boundary layer, fps

u local velocity within boundary layer, fps

V_o free-stream velocity, fps

v suction air velocity normal to outer surface of the airfoil, fps

X chordwise extent of porous area, ft

x distance from leading edge of the porous area measured parallel to chord line, ft

y distance from airfoil measured normal to surface, ft

α angle of attack, deg

γ ratio of specific heats for air, taken as 1.4

δ total boundary-layer thickness, ft

δ^* boundary-layer displacement thickness, $\int_o^\delta \left(1 - \frac{u}{U}\right) dy$, ft

θ boundary-layer momentum thickness, $\int_o^\delta \frac{u}{U}\left(1 - \frac{u}{U}\right) dy$, ft

τ index of resistivity defined as the total-pressure difference in in. H_2O required to induce a suction air velocity of 1 fps through a porous material of a given thickness

ρ mass density of air, slugs/cu ft

Subscripts

e	local external point
TE	trailing edge of porous area
o	free-stream conditions
1	conditions in suction duct
0.5	station, percent chord

MODEL

The model used for this investigation had a 4.5-foot chord and spanned the 7-foot dimension of the wind tunnel. The airfoil section was the NACA 0006. (Coordinates are given in table I.) Flush orifices were provided along the midspan of the model for determining the chordwise distribution of pressure. The model is shown installed in the wind tunnel in figure 1.

For the tests of the plain wing, a solid wood nose was used. Details of the model illustrating the arrangement of the permeable material in the porous nose are shown in figure 2. The permeable leading edge consisted of a perforated metal sheet backed with a commercial grade of felt. The characteristics of the perforated sheet and felt are given in table II. The perforated sheet formed the external airfoil surface and was spot-welded to 1/16-inch-thick ribs spaced approximately 4.5 inches. The felt was held against the perforated surface material by a 16-mesh, 0.023-inch-diameter wire cloth supported by 1/8-inch-diameter rods which passed through the metal ribs as shown in figure 2. The nose was porous from 2-percent chord on the lower surface around the leading edge to 7-percent chord on the upper surface. Various chordwise extents of porous area were obtained by closing off portions of the porous surface with a nonporous tape.

The thickness of the felt backing was varied to obtain various suction-velocity distributions. The chordwise variations of thickness and resistivity for the permeability arrangements tested are given in table III. The resistances to air flow of the porous materials are given in figure 3.

A 0.2-chord split flap was simulated in the tests by a 1/16-inch-thick metal plate fastened to the lower surface of the model and deflected 60° relative to the airfoil chord line with ribs between the flap and the model.

APPARATUS

The suction pressure required to induce flow through the porous material was provided by a vacuum pump located outside the wind tunnel. Air was drawn through the porous nose into the hollow spar in the airfoil and then through ducting and a control valve to the vacuum pump. The cross-sectional areas of the plenum chamber and ducting were large enough to reduce the dynamic pressure of the induced air to negligible values and to insure uniform internal pressure across the span of the model.

Boundary-layer velocity profiles were measured by means of small rakes fastened to the airfoil surface. A larger survey rake connected to an integrating manometer was used to measure wake pressures for the calculation of wake drag.

TEST METHODS

Air flow through the porous area of the airfoil was induced by maintaining a pressure inside the model that, generally, was less than the external pressure. The suction air velocity at a given chordwise station was calculated from the measured pressure difference across the porous material and the known flow-resistance characteristics of the porous materials. The flow-resistance characteristics of the porous materials were ascertained experimentally by the method described in reference 5. The section flow coefficients c_Q were calculated from integration of the suction air velocity across the porous surface.

The method of obtaining data was (1) to maintain various constant values of suction air velocity at a given chordwise point on the airfoil as the angle of attack was varied, or (2) to maintain various constant angles of attack as the suction air velocity was varied. For this latter method, at angles of attack above 6° there was a value of section flow coefficient below which a decrease in lift occurred as indicated in the adjacent sketch. The c_Q for a given angle of attack at which the decrease in lift occurs will hereafter be designated as the stall-point c_Q.

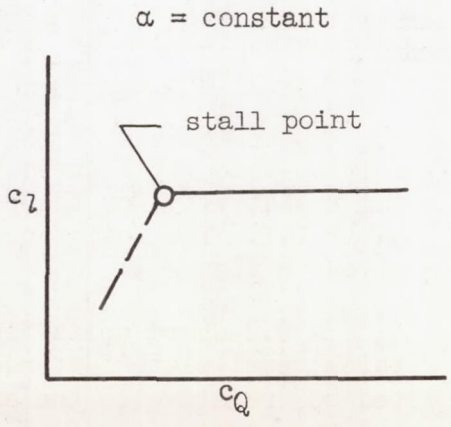

The tests covered a range of free-stream velocities from 93 to 187 fps (Mach number 0.07 to 0.17). The corresponding Reynolds number range based on the airfoil chord was 2.4 to 5.1 million. Wake-drag data were obtained at a Reynolds number of 5.1 million.

The lift and pitching moment were measured by the wind-tunnel balance system. The profile drag was calculated from wake pressures measured by a rake one-half chord length behind the trailing edge of the airfoil.

Tunnel-wall corrections computed by the method of reference 6 were applied to the data as follows:

$$\alpha = \alpha_u + 0.38\, c_{l_u} + 1.53\, c_{m_u}$$

$$c_l = 0.95\, c_{l_u}$$

$$c_d = 0.99\, c_{d_u}$$

$$c_m = 0.99\, c_{m_u} + 0.01\, c_{l_u}$$

where the subscript u denotes uncorrected values.

RESULTS AND DISCUSSION

Stall of the Model

In the present investigation, the use of area suction near the leading edge of the NACA 0006 airfoil increased the lift for angles of attack above 6° as shown in figure 4. The maximum lift coefficient of the plain airfoil without suction was 0.87 and the stall was of the thin-airfoil type described in reference 1. With the largest amount of suction that could be applied with the suction equipment ($c_Q = 0.0022$), the linear portion of the lift curve was extended to a lift coefficient of about 1.26 ($\alpha = 12°$). Above this lift coefficient, the lift continued to increase with increasing angle of attack, but at a considerably reduced rate, at least up to an angle of 19.5°. For angles of attack greater than 12°, the flow over the model as indicated by force, pressure-distribution, and boundary-layer measurements did not appear to be two dimensional. Tuft studies indicated a slight amount of rough flow on the model near the tunnel floor and ceiling at an angle of attack of about 10°. These regions of rough flow grew in extent, most rapidly near the trailing edge, with increasing angle of attack and covered a considerable portion of the model for angles of attack above 12°. Apparently the reduced pressure on the wing, especially with suction at high lifts, caused a transfer of some of the boundary layer from the tunnel walls on to the ends of the model. Attempts to eliminate or limit the spread of the region of rough flow with arrangements of separation plates, fences, and leading-edge slats at the ends of the model (similar to the arrangements used for the tests reported in refs. 3 and 4) were unsuccessful. Therefore, in the remainder of the report the discussion of the aerodynamic characteristics and flow requirements of the airfoil with suction will be limited to angles of attack less than about 12°.

For angles of attack less than 12°, the stall of the model, as the c_Q was reduced below the stall-point value, resembled thin-airfoil stall. The chordwise distributions of pressure showed an abrupt collapse of the leading-edge pressure peak with redistribution of the pressures giving the flat-type pressure-distribution characteristic of separated flow near the leading edge.

Effect of Chordwise Extent of Suction

The lift characteristics of the model with various chordwise extents of suction are shown in figure 5 for section flow coefficients above the stall-point values. The stall-point values of c_Q are listed in the following table for angles of attack near that at which an abrupt change in lift-curve slope occurred. Increasing the suction quantities above the stall-point values did not increase the lift significantly.

Chordwise extent of suction, percent c	α, deg	c_Q	c_l
0.3 lower to 2 upper	11.5	0.0020	1.23
0 to 7 upper only	11.5	.0049	1.24
0 to 1 upper only	11.5	.0008	1.22
0 to 0.5 upper only	11.5	.0006	1.22
0.1 to 2 upper only	9.4	.0015	1.00
0.2 to 2 upper only	8.4	.0012	.90

It was found that the minimum extent of suction required for lift control, 0- to 0.5-percent chord on the upper surface, also resulted in the least stall-point c_Q. This minimum extent is approximately the value determined by the method discussed by Thwaites in reference 7. Opening the porous area around the leading edge to the lower surface or downstream of 0.5-percent chord did not affect the lift at a given angle of attack but did increase the required volume of suction flow. The magnitude of the suction velocities between 0- and 0.5-percent chord at the stall point were, for all practical purposes, unchanged for openings greater than 0- to 0.5-percent chord.

The data in this report and those in reference 4 (leading-edge suction on an airfoil 10.5 percent thick) indicate that for both airfoils the optimum position of the leading edge of the porous area coincided with the location of the minimum external pressure coefficient.

Chordwise Variation of Suction Velocity

The lift and suction-flow characteristics of the model are shown in figures 6[1] and 7. The maximum values of c_Q shown in figures 6(a) and 7(a) were the maximum obtainable with the suction pump.

The data in figure 6 were obtained with a uniform thickness of felt backing the permeable surface material. With this arrangement, the pressure differences across the porous material induced suction velocities that were a minimum at the point of minimum external pressure and increased in magnitude for positions downstream as shown in figure 6(c). The data in figure 7 were obtained with the felt thickness tapered to give a nearly uniform suction velocity over the porous area at a lift coefficient of approximately 1.3 and a free-stream velocity of 162 fps.

Examination of parts (a) of figures 6 and 7 shows that the section flow coefficient to obtain a given lift coefficient was less for the tapered permeability. This can be seen more clearly in figure 8 where the variation of stall-point section flow coefficient with lift coefficient is presented for the two permeability arrangements. Although the stall-point suction-velocity distributions (parts (c) of figs. 6 and 7) differed, the plenum-chamber pressure coefficients at the stall point were nearly the same, as is shown in the following table:

α, deg	Stall-point plenum-chamber pressure coefficient, P_1	
	Uniform permeability	Tapered permeability
8.4	-13.1	-15.4
9.4	-18.0	-19.4
10.4	-22.8	-23.8
11.5	-27.5	-28.0
12.5	-31.4	-32.4

For the uniform permeability, the lift at a given angle of attack decreased when the suction velocity at the leading edge approached 0. The stall-point suction velocities at 0.5-percent chord increased with lift coefficient as shown in figure 9, and at a c_l of 1.3 were of the order of 2.5 percent of the local velocity outside the boundary layer.

[1]Data were first obtained with a less rigid surface material (see table II). With suction, a slight concavity formed between adjacent ribs. These data are not included, as the results were the same as those presented with the more rigid surface material which had no noticeable distortion.

For the tapered permeability, the stall-point suction velocities at 0.5-percent chord were considerably less than for the uniform permeability as shown in figure 9. At a lift coefficient of 1.3, the suction velocity was of the order of 2.0 percent of the local velocity at 0.5-percent chord.

Typical Aerodynamic Characteristics

The lift and pitching-moment characteristics are presented in figures 6(b) and 7(b). The profile drag of the model with the tapered permeability is shown in figure 10 for the suction-off and suction-applied cases. Two suction-off conditions are presented: (1) suction air line between the model and the suction pump closed and (2) porous area sealed with a nonporous tape between the porous metal surface and the felt backing.

The chordwise distributions of the external pressure coefficients on the plain airfoil and on the model with suction are shown in figure 11. For section flow coefficients above the stall-point value, the chordwise distributions of pressure were the same for either permeability distribution. The data in figure 11(a) illustrate the rapid development of high pressure peaks near the leading edge, typical of thin airfoils, as the angle of attack is increased. At 12° angle of attack with suction applied (fig. 11(b)), the pressure coefficient at the leading edge was approximately -30. The typical variation of the pressure distribution with decreasing section flow coefficient for a given angle of attack is shown in figure 11(c).

The variation of the pressure coefficients at various points on the chord with angle of attack are shown in figure 12. These data are typical for section flow coefficients from 0.0014 to 0.0022. It would appear, from the variation of pressure coefficient, that the flow phenomena which limited the gains in lift with suction to a lift coefficient of approximately 1.3 (discussed under "Stall of the Model") did not result from flow separation from the leading edge.

Velocities in the boundary layer were measured along the center of the span of the model from 10 to 95 percent of the chord on the upper surface. The results are presented in figure 13 as the chordwise variations of the derived parameters, momentum thickness θ, and shape parameter H. Typical boundary-layer velocity profiles from which these parameters were ascertained are shown in figure 14. With suction, the boundary layer at the trailing edge of the suction area could not be detected with a total-pressure tube (0.026-inch inside diameter and 0.005-inch wall) on the surface of the model until the suction velocities were reduced below the stall-point values.

The boundary-layer momentum thickness increased from the downstream edge of the suction area to the trailing edge of the airfoil. The shape

parameter H, however, remained nearly constant and was never greater than 1.7, even at 95-percent chord. This value is not considered to be indicative of separation of a turbulent boundary layer (ref. 8).

Effect of Free-Stream Velocity

In order to evaluate the power requirements for area suction it is necessary to stipulate the free-stream velocity as may be seen from the relation

$$\text{horsepower per foot of span} = \frac{c_w q_o V_o c}{550} \tag{1}$$

from reference 3, where c_w is a parameter not necessarily constant with free-stream velocity and is related to the section flow coefficient and plenum-chamber pressure coefficient by

$$c_w = -c_Q P_1 \left[1 - 0.6429 \left(\frac{P_1 q_o}{p_o} \right) + 0.4898 \left(\frac{P_1 q_o}{p_o} \right)^2 - 0.4023 \left(\frac{P_1 q_o}{p_o} \right)^3 \right] \tag{2}$$

For the 6-percent-thick airfoil investigated, the stall-point suction requirements were determined over a range of free-stream velocities from 93 to 187 fps. The results in terms of horsepower per foot of span are presented in figure 15 for the tapered permeability arrangement.

Over the Reynolds number range of the tests (2,400,000 to 5,100,000) for angles of attack above 8.4°, the horsepower per foot of span increased at a rate greater than V_o^3; this can be attributed to the increase in section flow and plenum-chamber pressure coefficients resulting from the increase in the stall-point suction velocities. The stall-point suction velocity at 0.5-percent chord generally increased more rapidly than V_o. The suction-velocity distributions corresponding to the stall-point suction velocities of figure 15 are presented in figure 16.

Effect of a Deflected Flap

The model was also tested with a 20-percent-chord split flap deflected 60° in order to obtain a high maximum lift at a more usable angle of attack. The results are shown in figure 17. The increase in lift-curve slope above 0° angle of attack for the model without suction with the flap deflected is characteristic of thin uncambered airfoils. The variation of lift coefficient with section flow coefficient and the stall-point suction-velocity distributions are presented in figure 18. Pressure-distribution diagrams are shown in figure 19.

Although the flow coefficients required to obtain the lift coefficients shown in figure 17 were not large, the external suction pressures against which the suction pump had to operate were very high, as shown in figure 19(b). At 12° angle of attack, the pressure coefficient at the leading edge was approximately -50. These low pressures tend to complicate the design of systems for area suction on the leading edges of thin wings. The variation of the pressure coefficients at various points on the chord with angle of attack are shown in figure 20.

Comparison with Stall-Point Suction Velocities for 10.5-Percent-Thick Airfoil

A comparison was made of the stall-point suction-velocity distributions on the 6-percent-thick airfoil (without the split flap) used in this investigation and on the symmetrical 10.5-percent-thick airfoil used for the research reported in reference 4. This comparison indicated that the values of the stall-point suction velocities at the trailing edge of the suction area were a function of the difference between the pressure coefficients at the leading and trailing edges of the porous areas. Such a relationship is useful for design purposes in that it provides a basis for estimating the stall-point section flow coefficient for airfoils with thickness-chord ratios in the range investigated.

For points downstream of approximately 3-percent chord, the external pressure coefficients were practically equal for the two airfoils at the same angle of attack. (See fig. 21.) Upstream of 3-percent chord, the pressure coefficients were more negative for the NACA 0006 airfoil. The differences between the pressure coefficients at the leading and trailing edges of the porous areas are presented in figure 22 for the NACA 0006 airfoil and the 10.5-percent-thick airfoil. The data in this figure are for chordwise extents of suction from 0- to 0.5-percent chord and 0- to 1-percent chord for the NACA 0006 airfoil and from 0.3- to 3-percent chord for the 10.5-percent-thick airfoil.

In figure 23, the variations of the lift increment above the maximum for the plain wings and the ratio of suction to local velocity at the trailing edge of the suction area are presented as functions of the difference in pressure coefficient between the leading and trailing edges of the porous area for the two airfoils. Included in this figure are data for the NACA 0006 airfoil for two chordwise extents of suction, for free-stream velocities from 93 to 187 fps, and with a deflected flap. It appears from the data of figure 23 that the required minimum suction-velocity ratios at the trailing edge of the porous area are a function of the pressure-coefficient difference between the leading and trailing edges of the porous area. This relationship appears to be independent of the chordwise extent of suction or the free-stream velocity and also appears to apply to the minimum suction velocities required for the

airfoil with a deflected flap. However, the lift increments obtained with the deflected flap were less for a given pressure difference across the porous area.

The suction-velocity distributions for two of the permeability arrangements of figure 23 at a free-stream velocity of 162 fps and a ΔP_e of 14.4 are shown in figure 24. In reference 4, it was shown that the suction velocity at the leading edge of the suction area could be reduced below that for arrangement K and still maintain the same value of lift coefficient, provided that the suction velocity at the trailing edge of the suction area was maintained (as is shown by the data for arrangement L in figure 24). It is believed that with the proper chordwise distribution of τ to yield a suction-velocity distribution corresponding to that indicated by the dashed line (fig. 24), the stall-point c_Q values for the airfoil of this investigation could be reduced for the same plenum-chamber pressures. For the minimum chordwise opening from 0- to 0.5-percent chord, it is estimated that the value of c_Q to attain a lift coefficient of 1.27 would be 0.0003. With the same suction-velocity distribution being assumed through the first 0.5-percent chord but with the downstream edge of the porous area extended to 1.0-percent chord, the value of c_Q to obtain the same lift would be 0.0007. For comparison with the test results, the calculated minimum suction quantities are presented in figure 8.

DESIGN CONSIDERATIONS

Analysis of the results of this investigation and the two-dimensional tests reported in references 2, 4, and 9 indicate certain parameters to be considered in applying area suction to airfoils to prevent or delay leading-edge flow separation. These design considerations are purely empirical and are based on tests of conventional round-nosed airfoils whose maximum lift without suction is limited by flow separation from the leading edge. The design considerations also seem to apply, at least as a first approximation, to airfoils with a flap.

Lift Increment Due to Suction

With leading-edge area suction, the increase in section lift coefficient above that of the plain airfoil obtained for several airfoils of different thickness were as follows:

Reference	$\frac{t}{c}$	$c_{l_{max}}$ of plain airfoil	Δc_l due to suction	Test Reynolds number, million
2	0.12	1.27	0.36	1.5
4	.105	1.30	.45	4.5
9	.08	.89	.40	.3
---	.06	.87	.40	4.5
---	.06 with .2-chord split flap $\delta = 60^\circ$	1.89	.43	4.5

Although in each case the increment of lift obtained with suction was about 0.4, it should be pointed out that for the 10.5- and 12-percent thick airfoils, maximum lift was limited by turbulent flow separation which started from the trailing edge. For the 6- and 8-percent-thick airfoils the lift increment due to suction appeared to be limited by flow separation resulting from tunnel-wall boundary-layer interference.

Location and Extent of Suction Area

The upstream edge of the porous opening should be on the upper surface at the point of minimum pressure. The downstream edge should be where the external pressure coefficient corresponding to the desired lift coefficient is no greater than the minimum pressure coefficient reached prior to the stall on the airfoil without suction. Increasing the chordwise extent beyond this minimum length does not increase the magnitude of the lift obtained but does increase the suction quantity required for a given lift.

Suction-Velocity Distribution

The suction-velocity distribution should be designed for the highest operating free-stream velocity to be encountered at the design lift coefficient. The chordwise distribution of the suction velocity to obtain maximum lift with minimum suction quantity should increase from approximately zero at the upstream edge of the suction area to a value at the downstream edge which is dependent on the free-stream velocity and the difference between the external pressure coefficients at the leading and trailing edges of the suction area. The values of suction-velocity ratio at the downstream edge of the porous area for various free-stream velocities can be estimated from figure 35 of reference 4 and figures 15 and 23 of this report.

Selection of Porous Material

The resistivity of the porous material at the upstream edge of the porous area should be small in order to keep the suction pressures as small as possible. The value of τ should increase downstream sufficiently to obtain the required suction velocity at the downstream edge of the suction area at the design free-stream velocity and lift coefficient.

The type of porous material can be selected with the aid of reference 5. The surface texture, sintered metal or perforated plate (700 to 4,200 holes/sq in.), is not a controlling factor for maximum lift.

Power Requirements

The power required for suction, neglecting duct losses, can be calculated from the external pressure distribution, the plenum-chamber pressure, and the flow resistance of the porous material. (See ref. 3 for sample calculations.) The calculations would not be dependent on the material itself but rather on the index of resistivity τ of the material.

CONCLUDING REMARKS

Two-dimensional tests were made of an NACA 0006 airfoil with area suction near the leading edge. Aerodynamic data and suction requirements were obtained for various chordwise extents of suction within the region from 2-percent chord on the lower surface around the leading edge to 7-percent chord on the upper surface at free-stream velocities between 93 and 187 fps. At a free-stream velocity of 162 fps, a section flow coefficient of 0.0010 increased $c_{l_{max}}$ from about 0.87 to 1.25 by delaying the stall from 9° to 12° angle of attack. The most economical extent of suction for this lift increase was on the upper surface from the leading edge to 0.5-percent chord.

Data were also obtained with a 0.2-chord split flap deflected 60°. With this flap, a section flow coefficient of 0.0015 at a free-stream velocity of 133 fps increased $c_{l_{max}}$ from 1.9 to 2.2.

High negative values of pressure coefficient were obtained on the leading edge of the airfoil with suction. Pressure coefficients of the order of -30 and -50 were obtained for the airfoil and for the airfoil with the split flap deflected 60°, respectively. These low pressures which the pump must supply tend to complicate the design of systems for area suction.

From a comparison of the results obtained on the NACA 0006 airfoil in this investigation with the results obtained on a symmetrical airfoil 10.5 percent thick (NACA TN 3093), it was found that for a given lift increase the minimum suction quantity required was related to the magnitude of the difference between the external pressure coefficients at the leading and trailing edges of the porous area.

Ames Aeronautical Laboratory
National Advisory Committee for Aeronautics
Moffett Field, Calif., June 29, 1954

REFERENCES

1. McCullough, George B., and Gault, Donald E.: Examples of Three Representative Types of Airfoil-Section Stall at Low Speed. NACA TN 2502, 1951.

2. Nuber, Robert J., and Needham, James R., Jr.: Exploratory Wind-Tunnel Investigation of the Effectiveness of Area Suction in Eliminating Leading-Edge Separation Over an NACA 64_1A212 Airfoil. NACA TN 1741, 1948.

3. Dannenberg, Robert E., and Weiberg, James A.: Section Characteristics of a 10.5-percent-Thick Airfoil With Area Suction as Affected by Chordwise Distribution of Permeability. NACA TN 2847, 1952.

4. Dannenberg, Robert E., and Weiberg, James A.: Effect of Type of Porous Surface and Suction Velocity Distribution on the Characteristics of a 10.5-Percent-Thick Airfoil With Area Suction. NACA TN 3093, 1953.

5. Dannenberg, Robert E., Weiberg, James A., and Gambucci, Bruno J.: The Resistance to Air Flow of Porous Materials Suitable for Boundary-Layer-Control Applications Using Area Suction. NACA TN 3094, 1954.

6. Allen, H. Julian, and Vincenti, Walter G.: Wall Interference in a Two-Dimensional-Flow Wind Tunnel, With Consideration of the Effect of Compressibility. NACA Rep. 782, 1944.

7. Thwaites, B.: A Theoretical Discussion of High Lift Aerofoils with Leading-Edge Porous Suction. R. & M. No. 2242, British A.R.C., 1949.

8. von Doenhoff, Albert E., and Tetervin, Neal: Determination of General Relations for the Behavior of Turbulent Boundary Layers. NACA Rep. 772, 1943.

9. Pankhurst, R. C., Raymer, W. G., and Devereux, A. N.: Wind Tunnel Tests of the Stalling Properties of an 8% Thick Symmetrical Section with Continuous (Distributed) Nose Suction. R. & M. No. 2666, British A.R.C., 1948.

10. Anon.: General Catalog No. 62, Perforated Materials, The Harrington and King Perforating Company, Chicago, Ill., 1950.

11. Anon.: Data Sheet No. 5, The American Felt Co., Glenville, Conn., 1947.

12. Anon.: Lektromesh Specification Sheet, The C. O. Jelliff Mfg. Corp., Southport, Conn., 1949.

TABLE I.- COORDINATES OF THE NACA 0006 AIRFOIL
[Percent airfoil chord]

Station	Ordinate
0	0
1.25	.95
2.5	1.31
5.0	1.78
7.5	2.10
10	2.34
15	2.67
20	2.87
25	2.97
30	3.00
40	2.90
50	2.65
60	2.28
70	1.83
80	1.31
90	.72
95	.40
100	(.06)
100	0
L.E. radius:	0.40

TABLE II.- CHARACTERISTICS OF THE MATERIALS USED IN THE POROUS LEADING EDGE

Surface: Perforated metal sheet (ref. 10)	
Hole diam., in.	0.020
Holes per sq in.	714
Percent open	23.0
Nominal thickness, in.	0.016
Index of resistivity, τ	0.009
Backing: Felt cloth (ref. 11)	
Color	white
lb/sq yd	8.4
Percent wool	100
Nominal thickness, in.	0.50
Index of resistivity, τ	
for 0.15 in. thickness	3.6
for 0.50 in. thickness	8.2

Data were also obtained but not presented in this report for the model equipped with a surface material consisting of a 0.006-inch-thick metal mesh having 4,225 0.005-inch square perforations per sq in. and 10.5-percent open area (ref. 12).

TABLE III.- PERMEABILITY ARRANGEMENTS TESTED

Chordwise station, x/c, percent	Felt thickness in.	Index of resistivity, τ
Uniform permeability		
0 .10 .28 .60 1.17 2.00 2.92 5.75	0.15 ↓	3.6 ↓
Tapered permeability		
0	0.062	1.04
.10	.135	2.07
.28	.22	3.55
.60	.30	4.88
1.17	.37	6.01
2.00	.41	6.57
2.92	.44	7.22
5.75	.48	7.81

Figure 1.- The NACA 0006 airfoil with a porous leading edge.

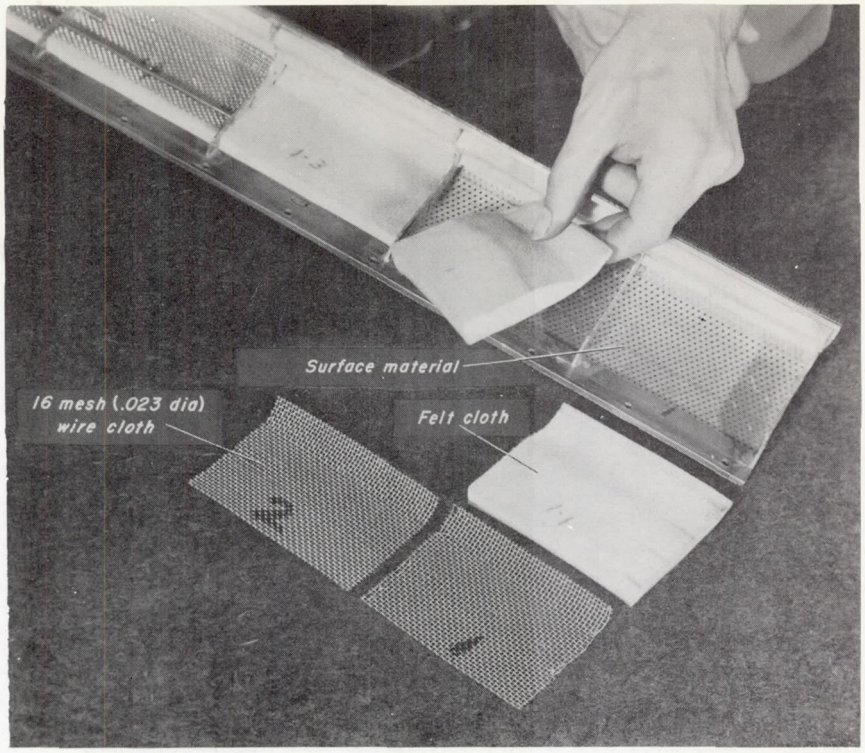

A-18010.1

(a) Arrangement of the permeable material in the leading edge.

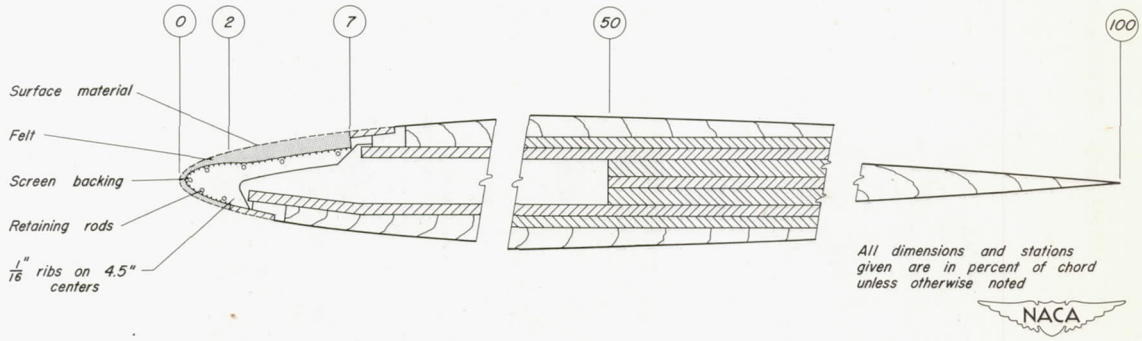

(b) Section through the model.

Figure 2.- Details of model construction.

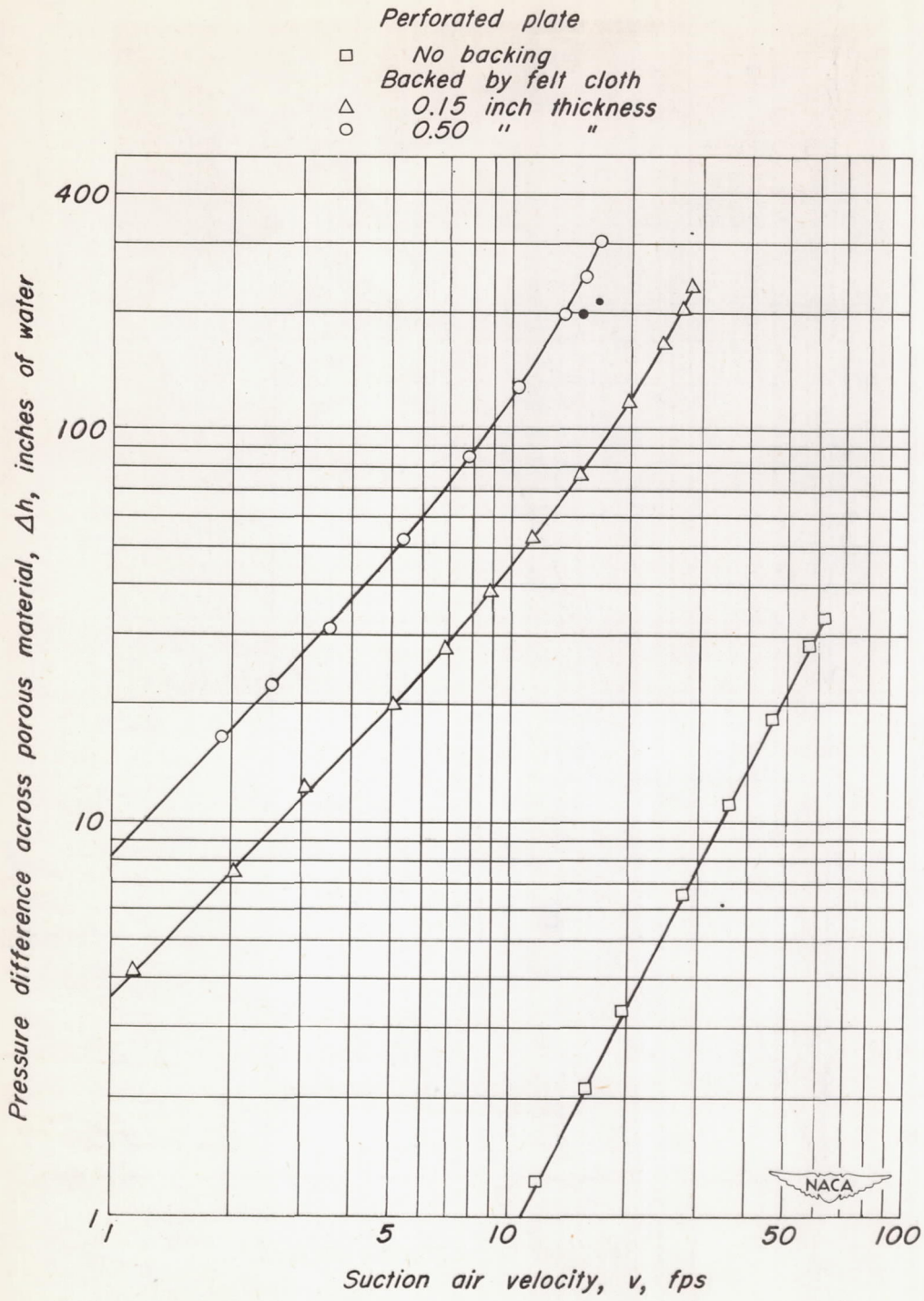

Figure 3.- Resistance to air flow of the porous materials used in the tests.

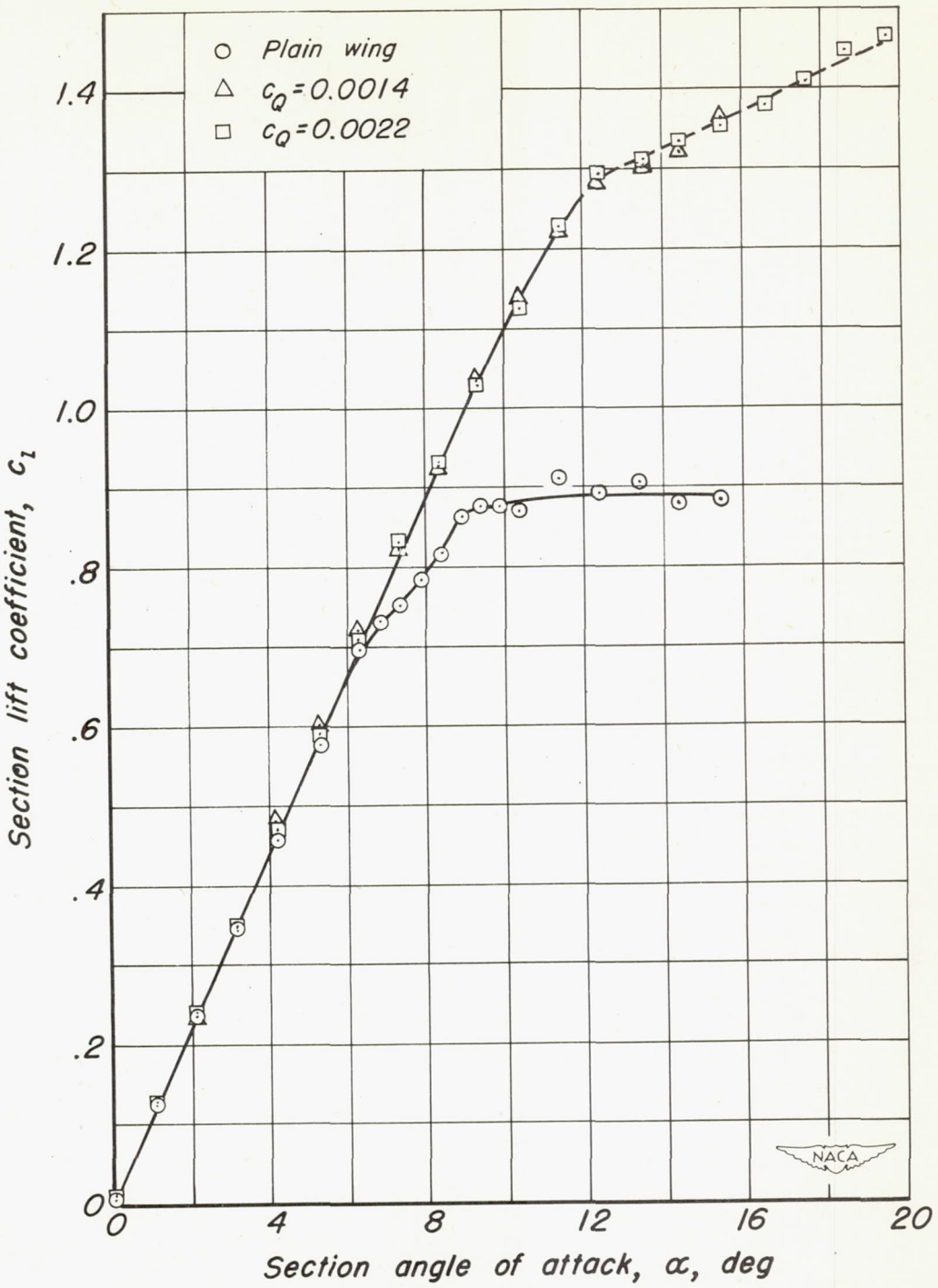

Figure 4.- Effect of suction on the lift characteristics of the model; $V_o = 162$ fps.

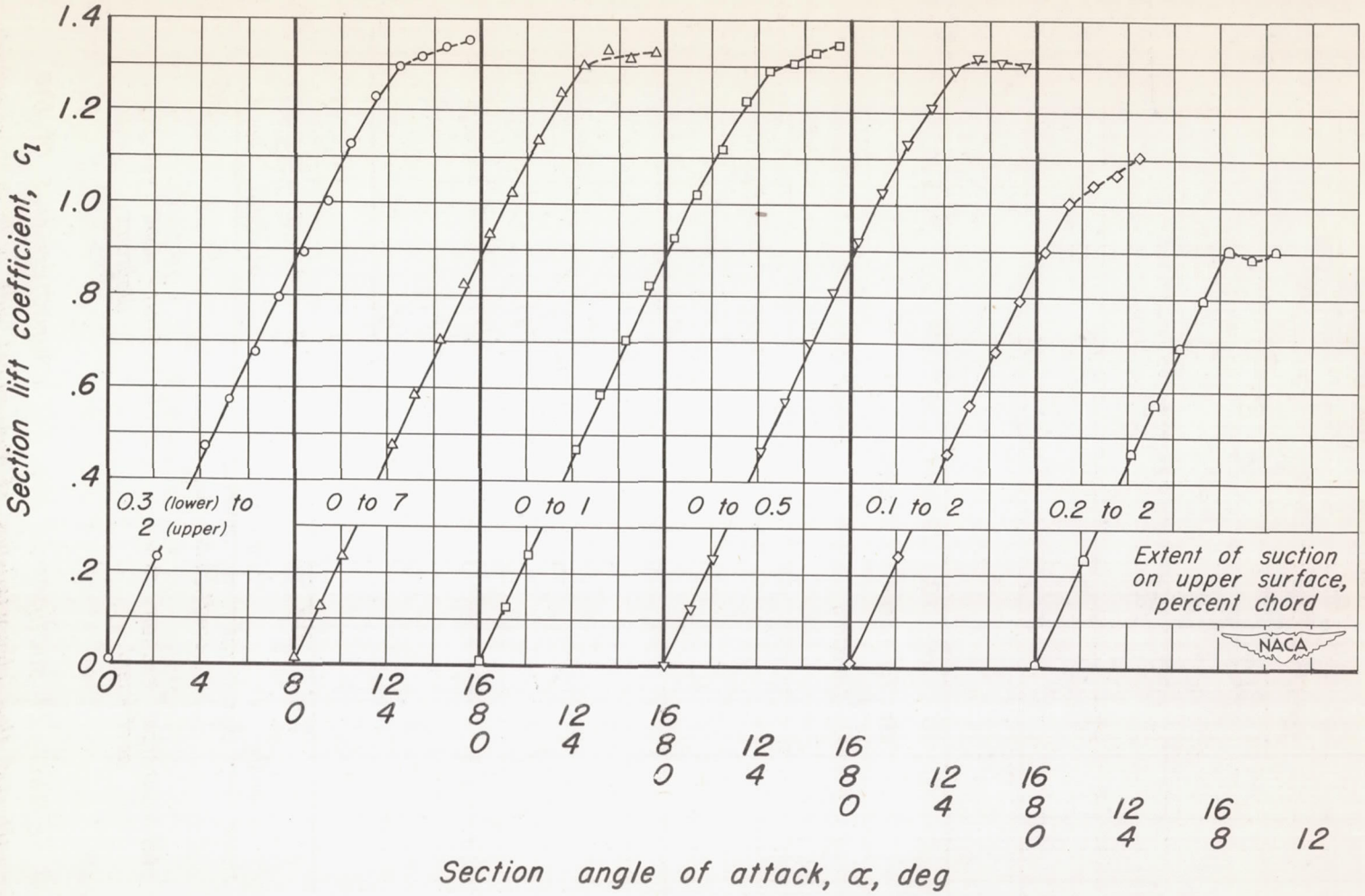

Figure 5.– Lift characteristics of the model for various chordwise extents of suction with the tapered permeability for section flow coefficients above the stall-point values; $V_0 = 162$ fps.

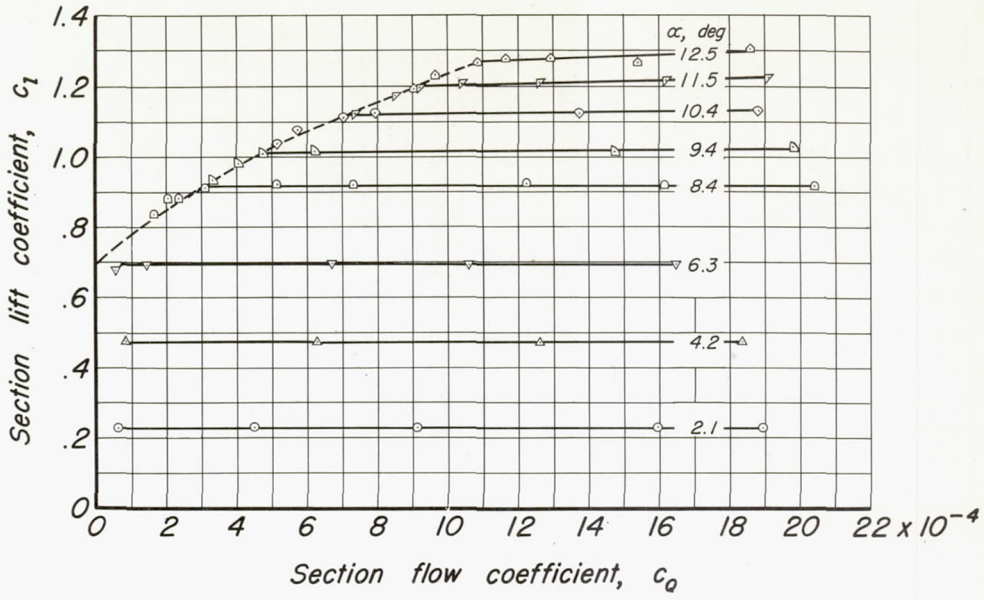

(a) Constant angle of attack.

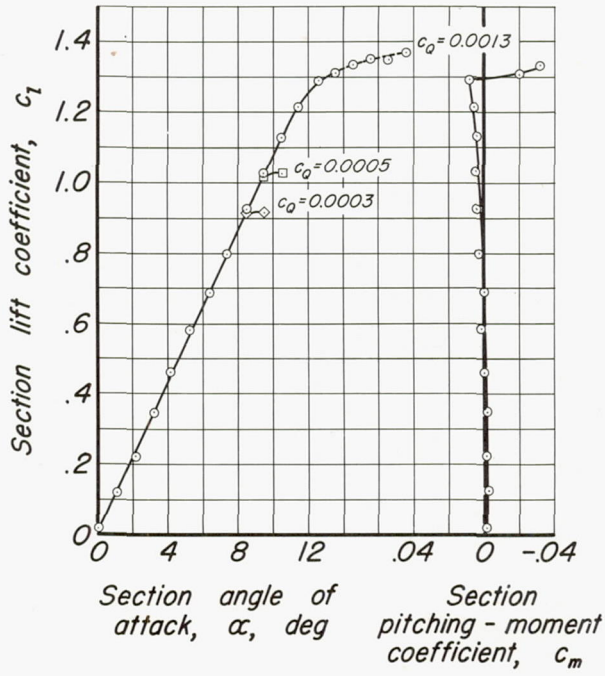

(b) Constant section flow coefficient.

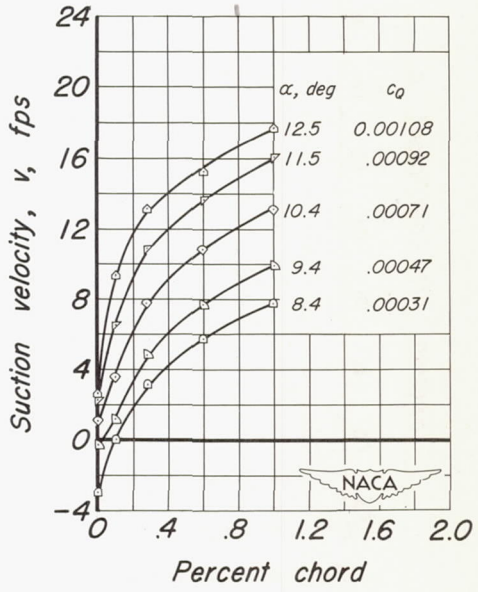

(c) Stall-point velocity diagrams.

Figure 6.- Lift and flow characteristics of the model with uniform permeability from 0- to 1-percent chord on the upper surface; V_0 = 162 fps.

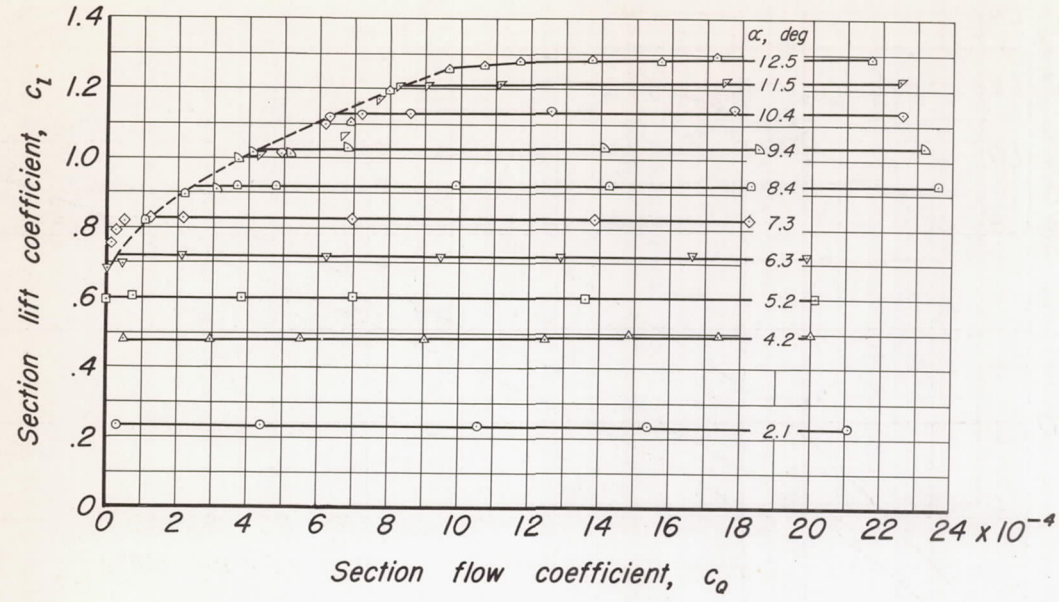

(a) Constant angle of attack.

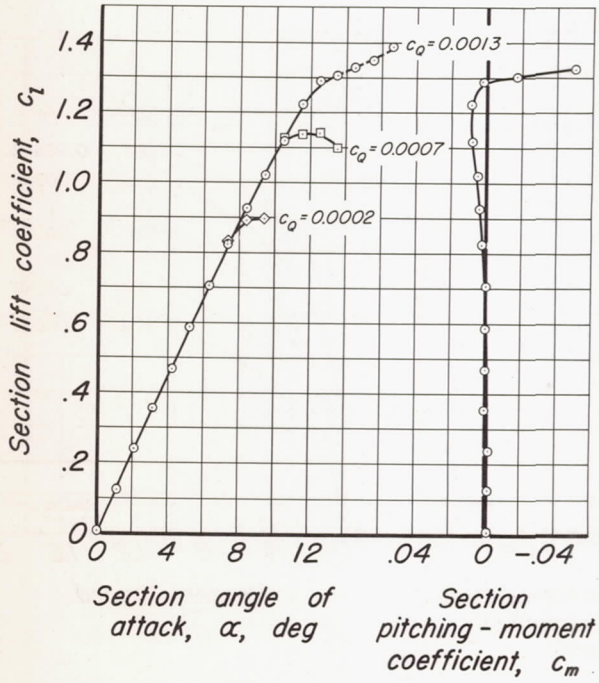

(b) Constant section flow coefficient.

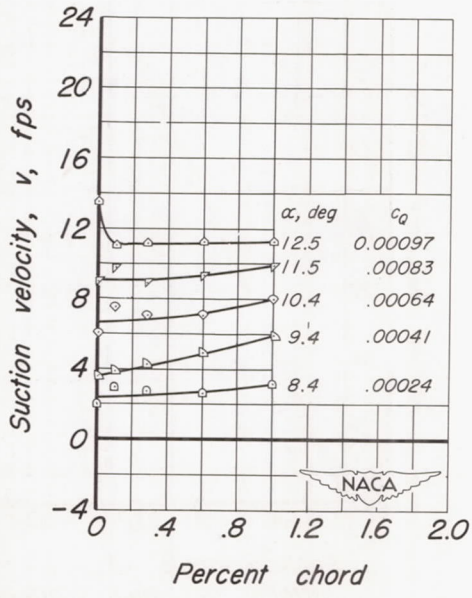

(c) Stall-point velocity diagrams.

Figure 7.- Lift and flow characteristics of the model with tapered permeability from 0- to 1-percent chord on the upper surface; V_0 = 162 fps.

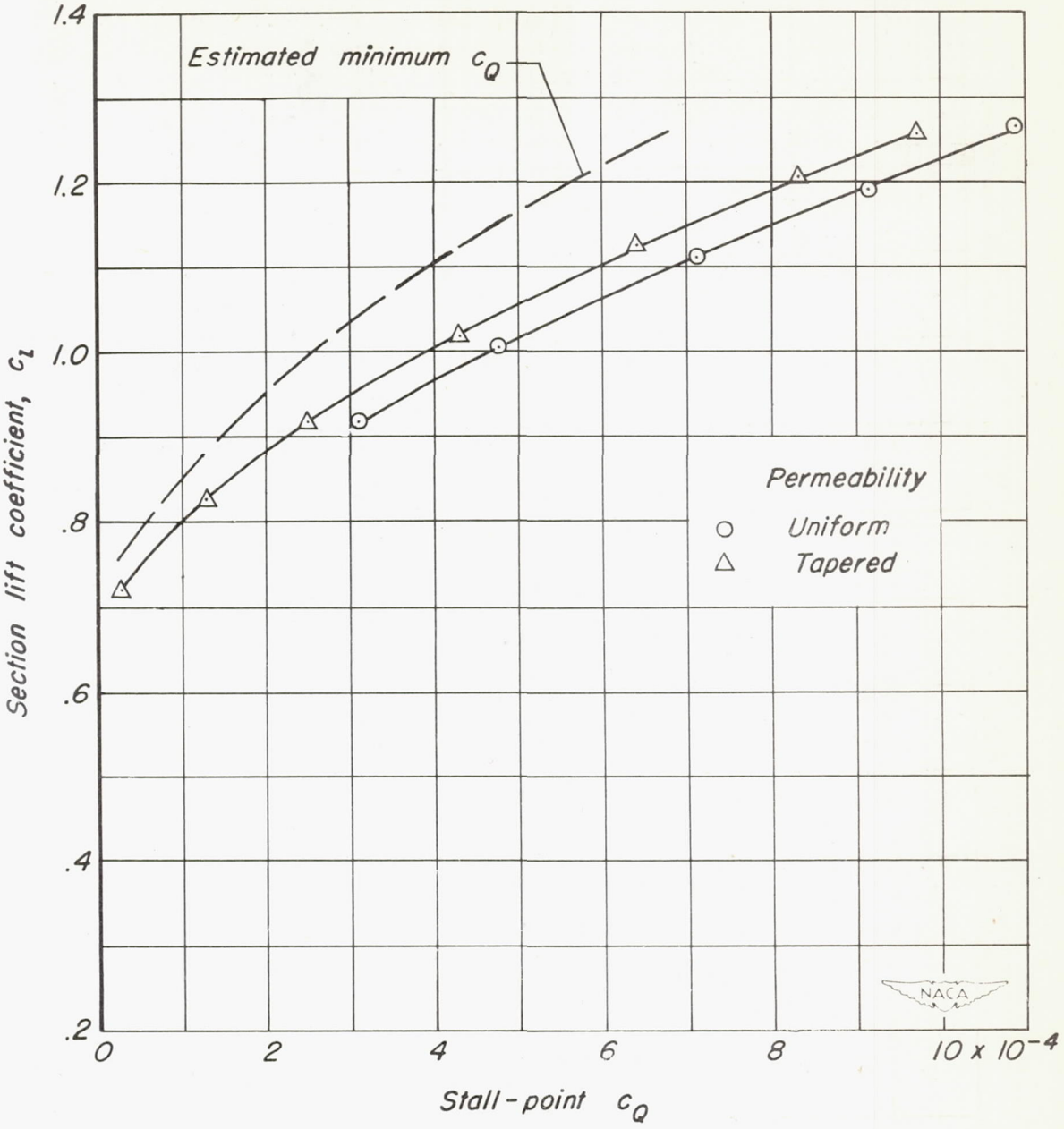

Figure 8.- Comparison of the stall-point section flow coefficients for the permeability arrangements tested, suction from 0-to 1-percent chord; V_0 = 162 fps.

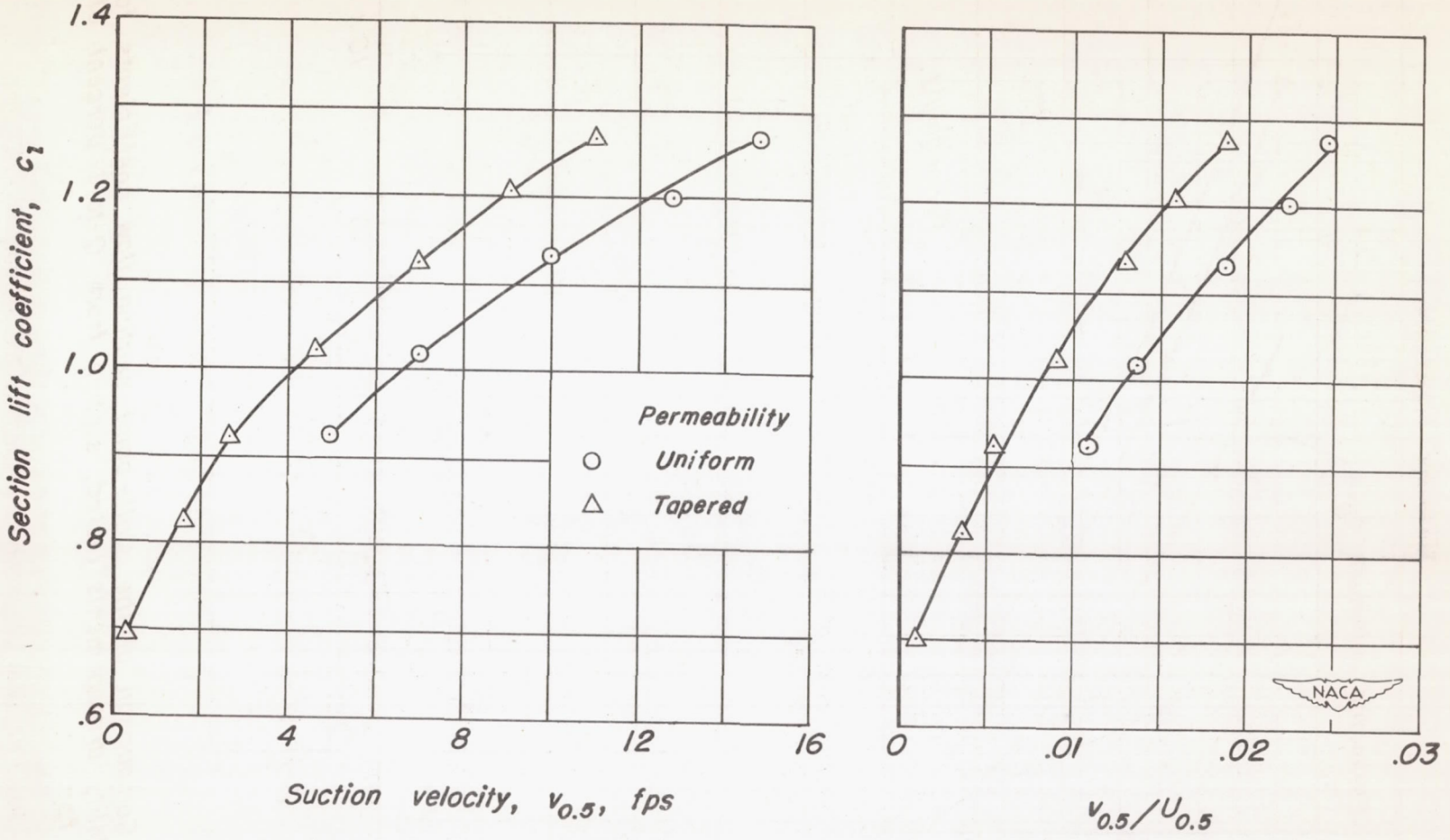

Figure 9.- Variation of the stall-point suction velocity at 0.5-percent chord with section lift coefficient, suction from 0- to 1-percent chord; $V_0 = 162$ fps.

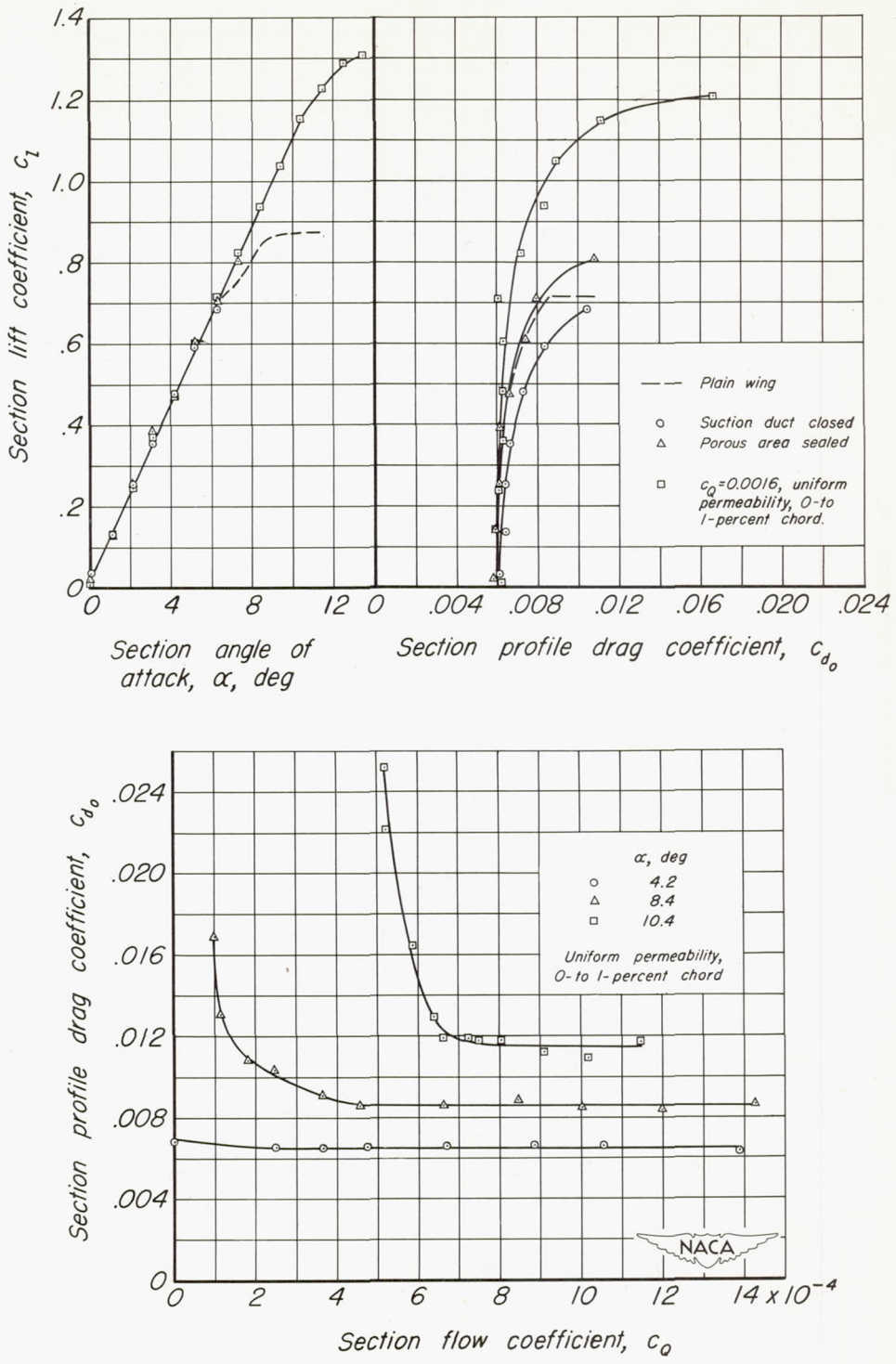

Figure 10.- Lift and drag characteristics of the model; V_o = 187 fps.

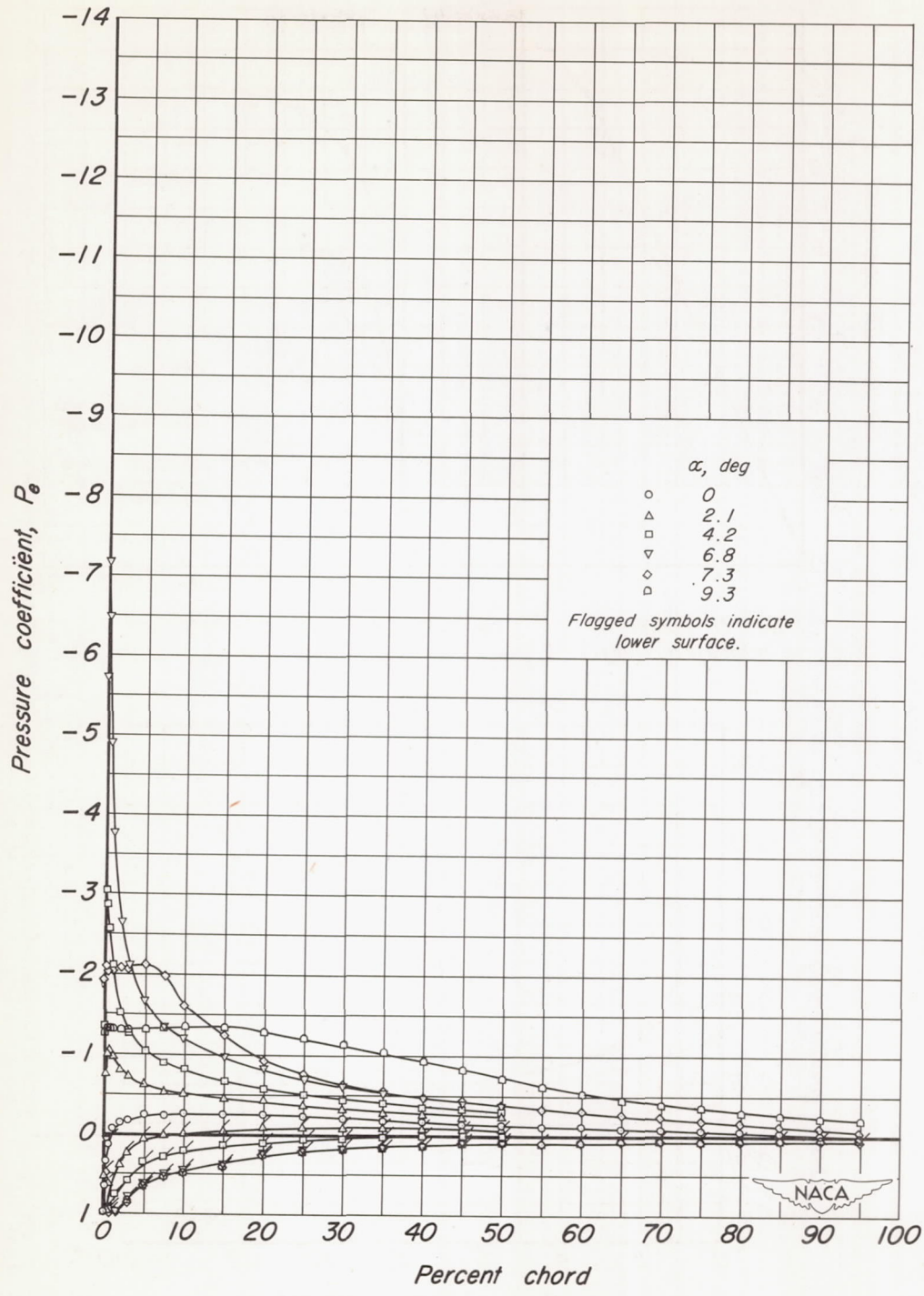

(a) Plain airfoil.

Figure 11.- Pressure distribution over the model; V_o=162 fps.

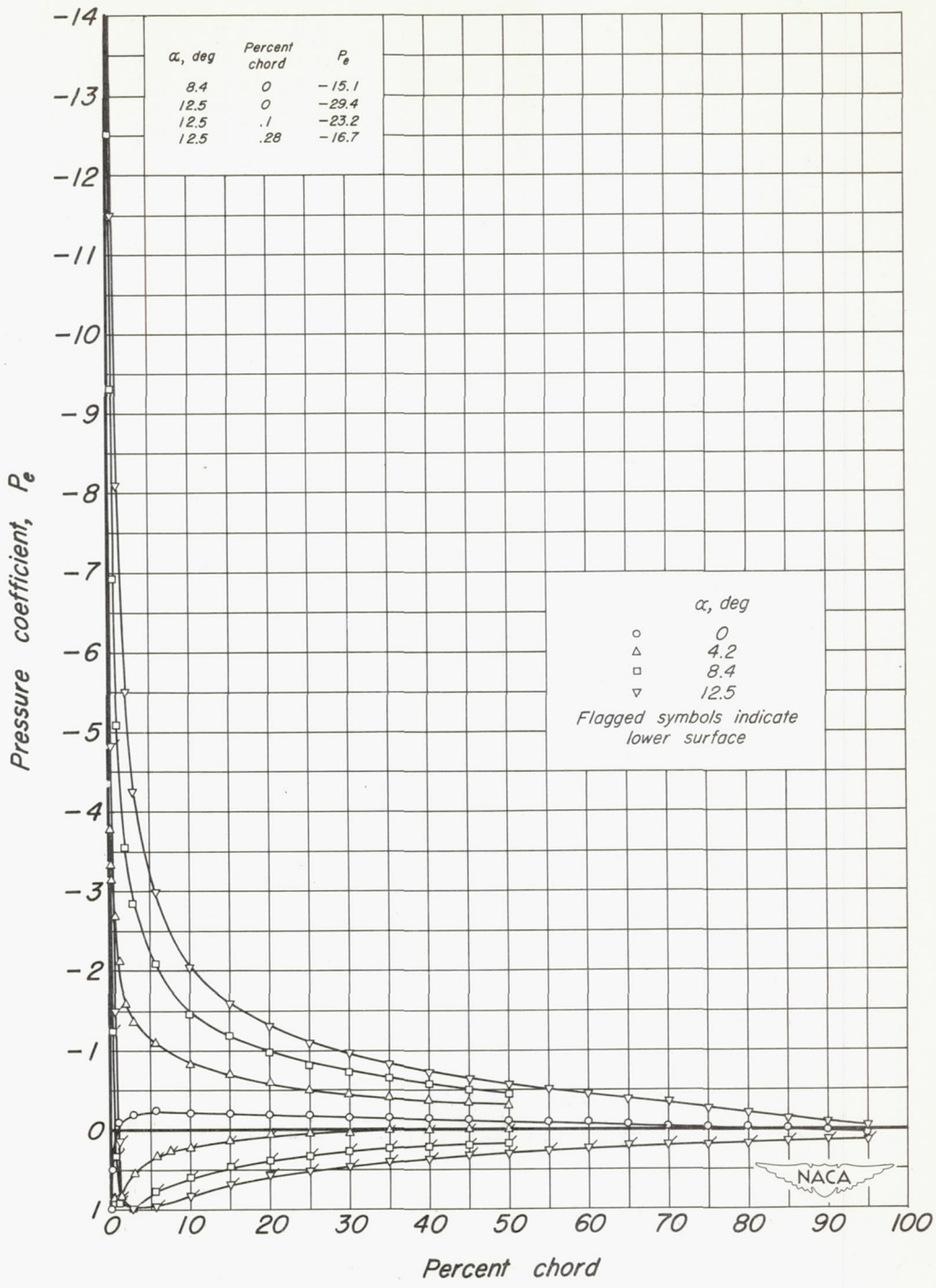

(b) Model with tapered permeability from 0-to 1-percent chord; c_Q=0.0016.

Figure 11.- Continued.

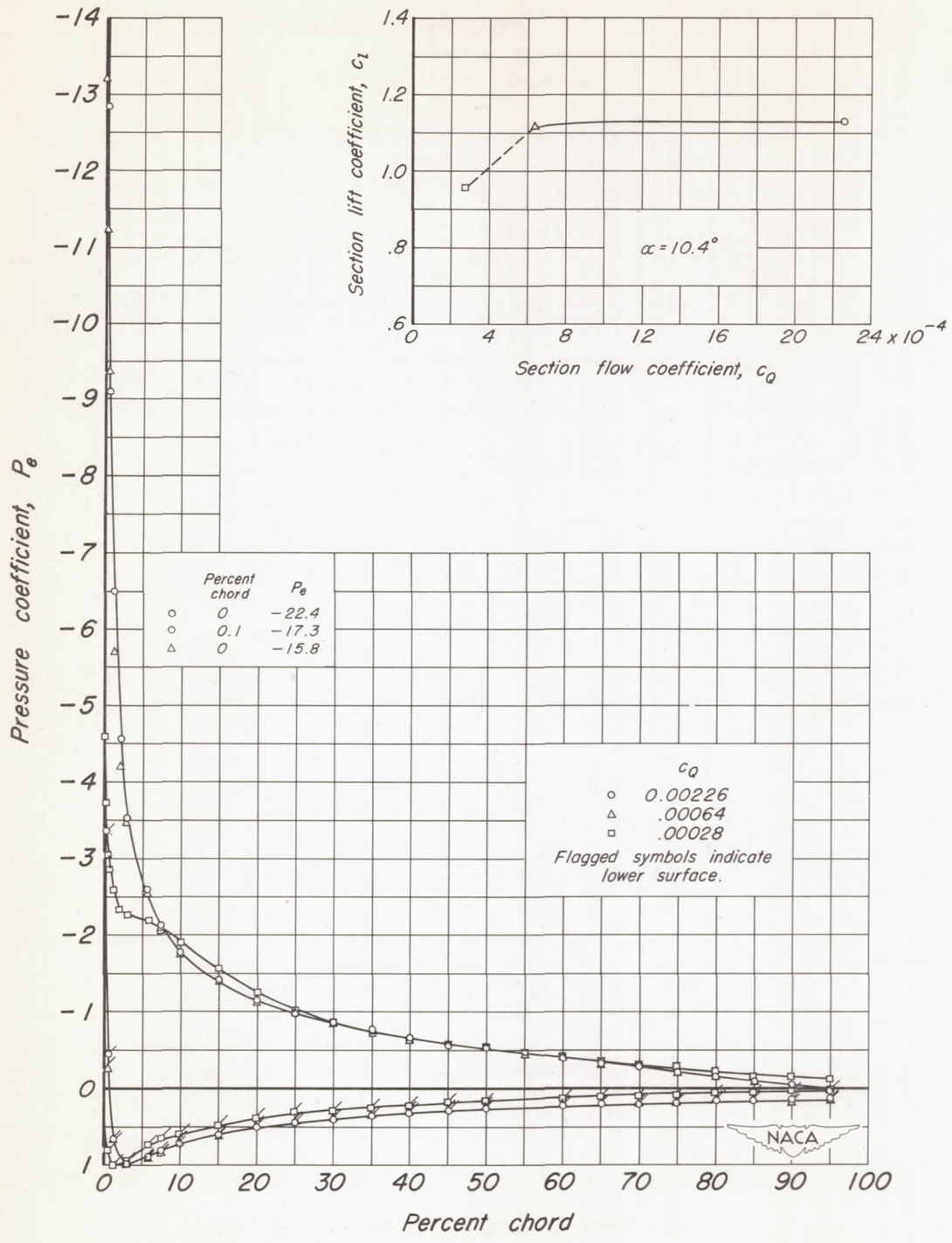

(c) Model with tapered permeability from 0-to 1-percent chord; $\alpha = 10.4°$.

Figure 11.- Concluded.

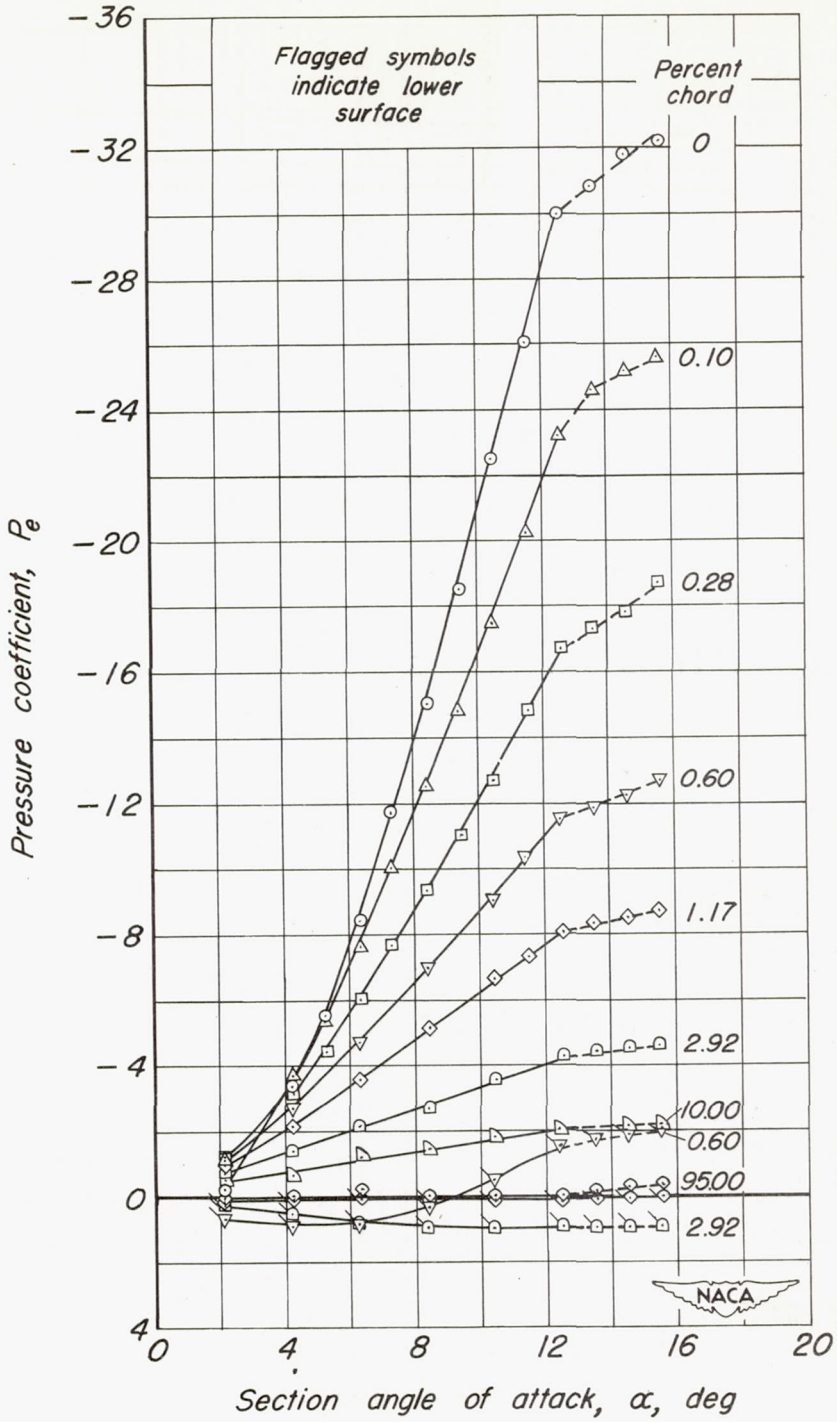

Figure 12.- Variation of the pressure coefficients at particular chordwise stations with angle of attack for the model with tapered permeability from 0- to 1-percent chord; c_Q=0.0016; V_0=162 fps.

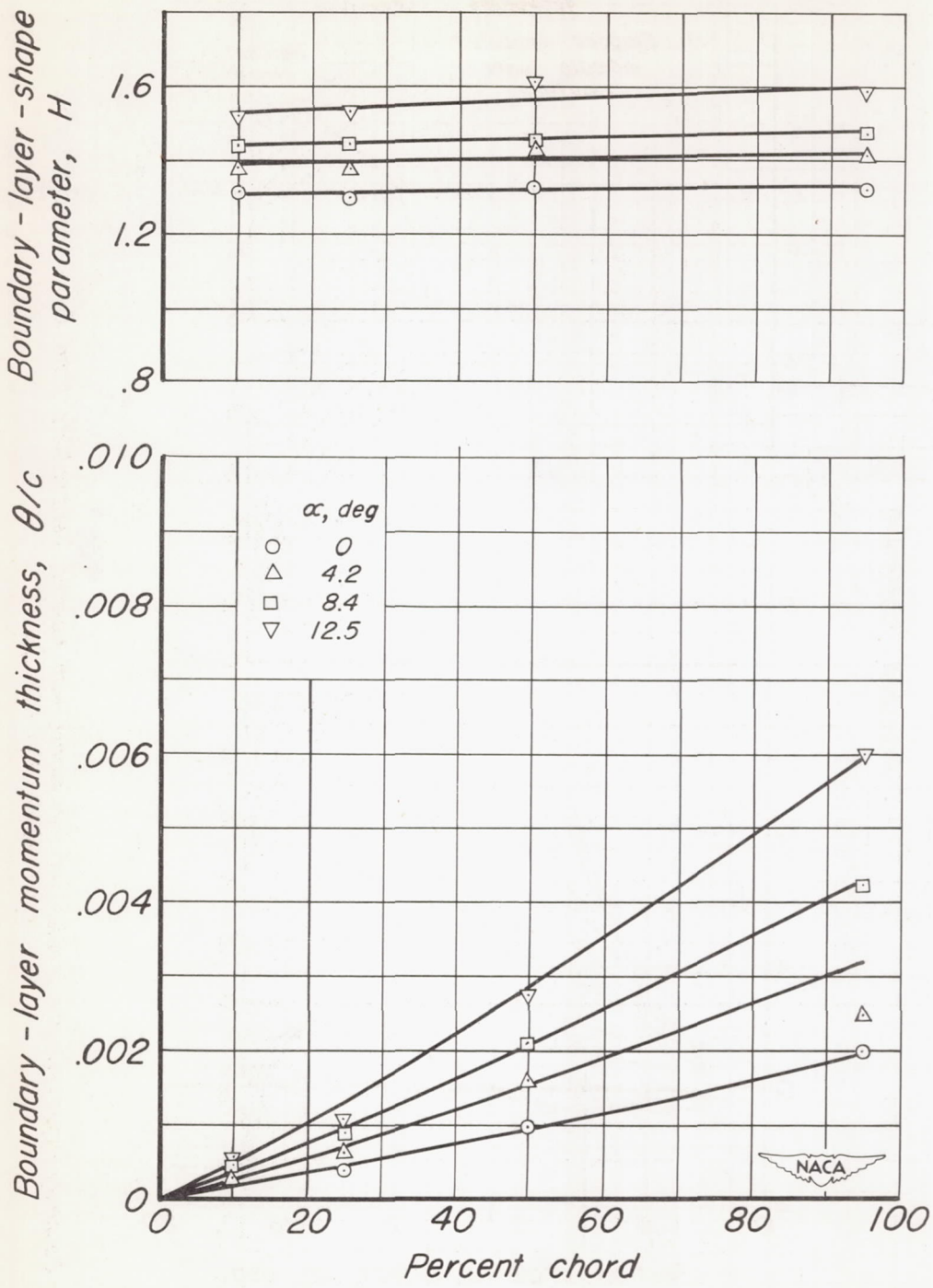

Figure 13. - Boundary - layer parameters for the model with tapered permeability from 0- to 1-percent chord; c_Q = 0.0016; V_0 = 162 fps.

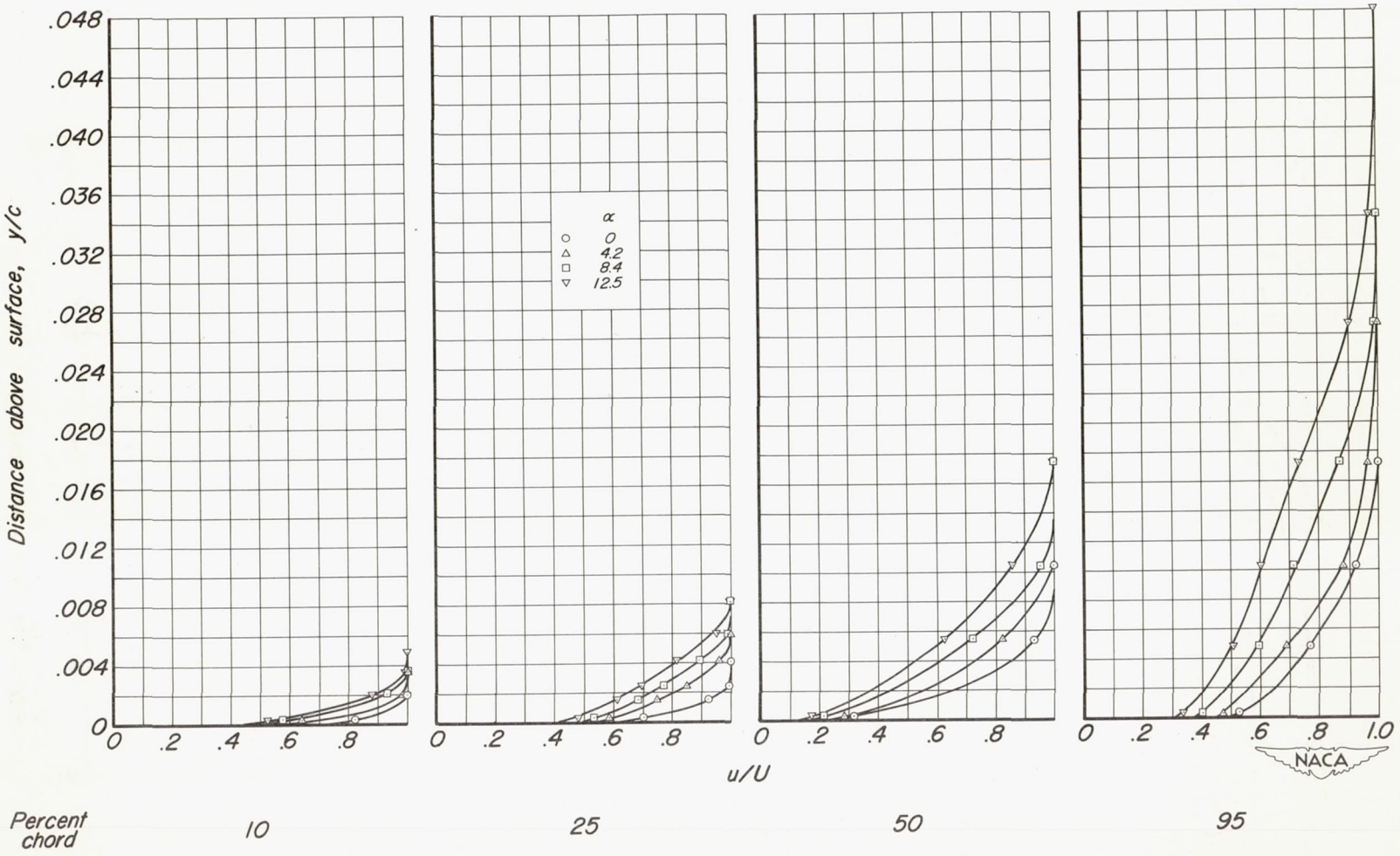

Figure 14.- Boundary-layer velocity profiles for the model with tapered permeability from 0-to 1-percent chord; $c_Q = 0.0016$; $V_0 = 162$ fps.

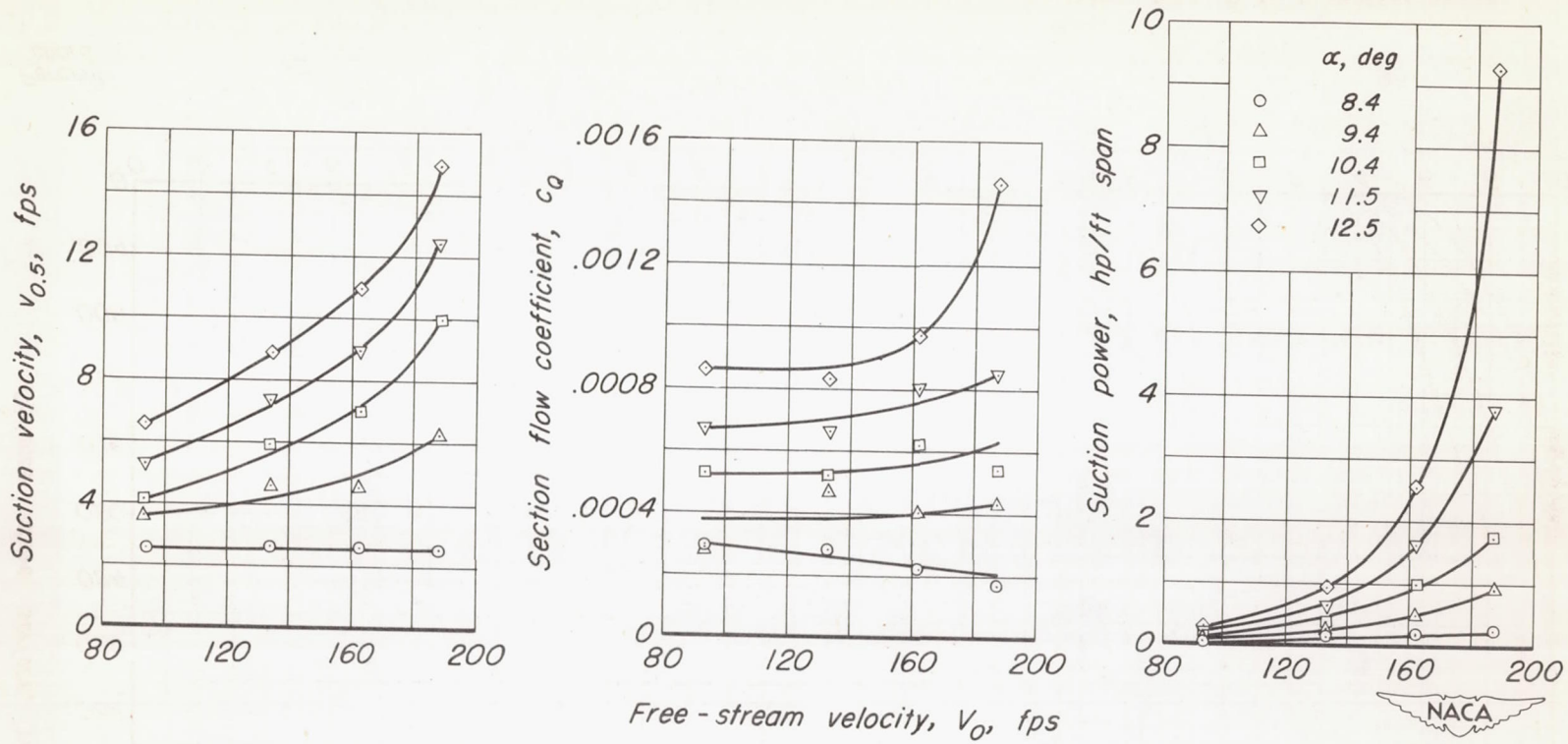

Figure 15.- Effect of free-stream velocity on the stall-point suction requirements of the model with tapered permeability from 0- to 1-percent chord.

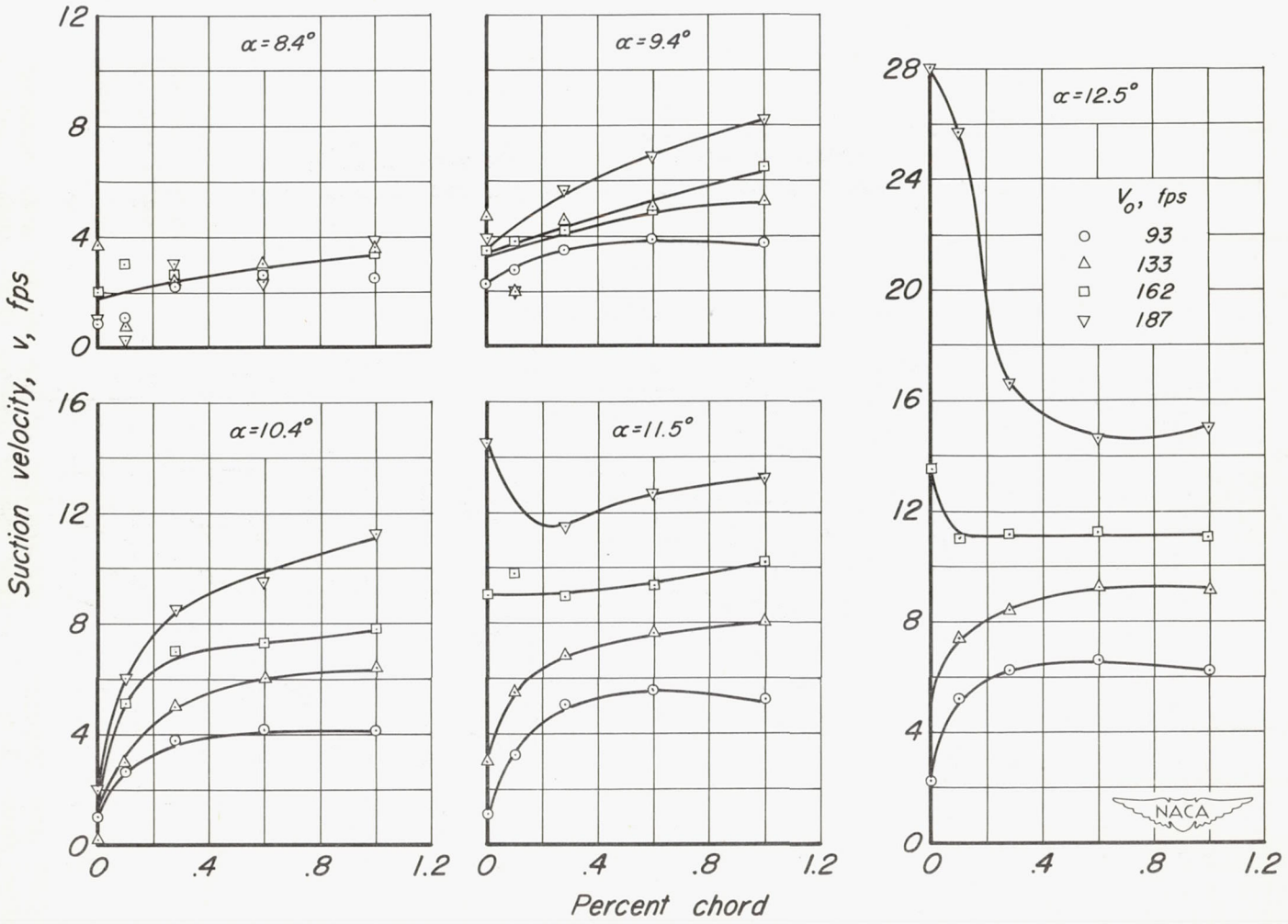

Figure 16.- Effect of free-stream velocity on the stall-point suction-velocity distribution for the model with tapered permeability from 0- to 1-percent chord.

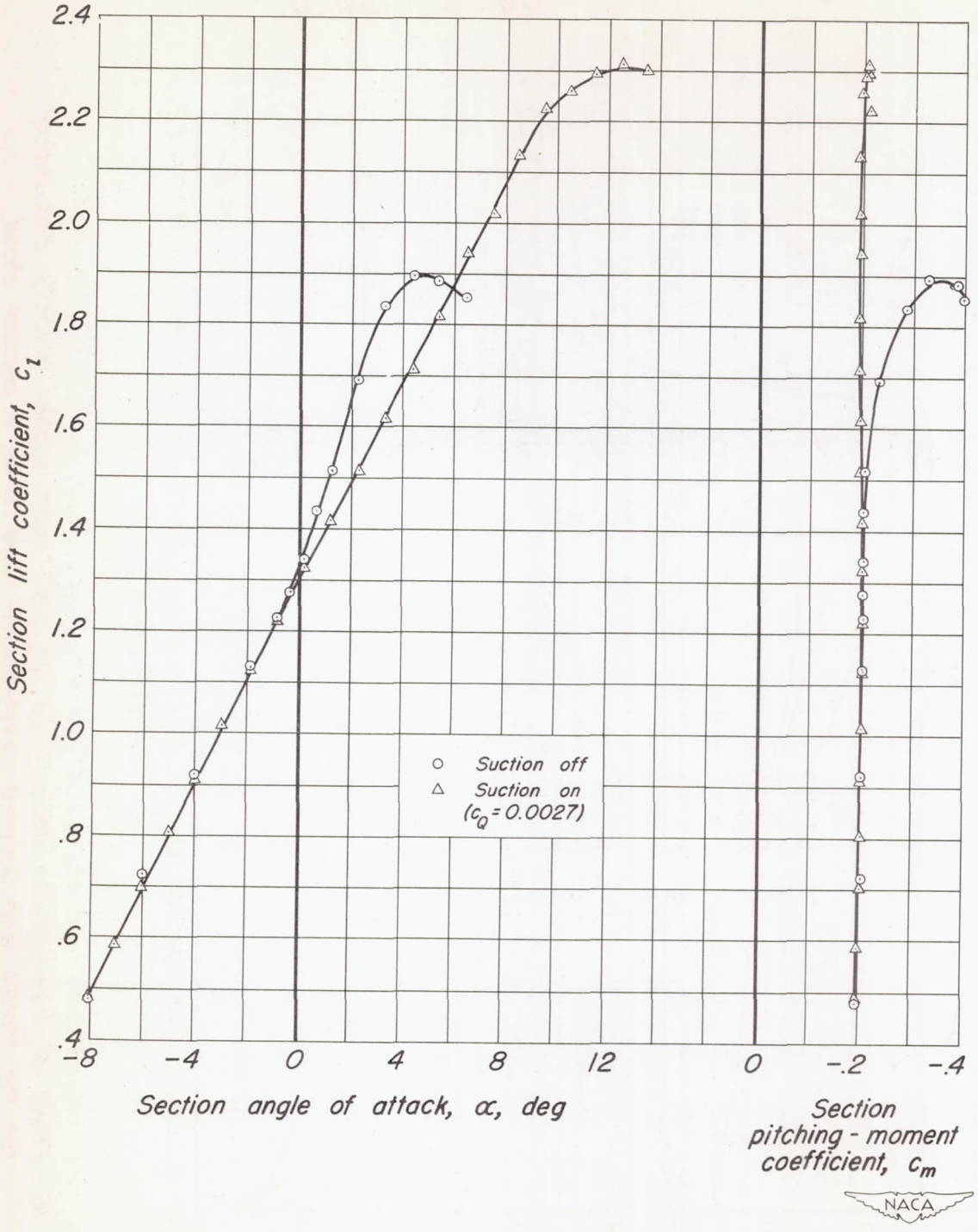

Figure 17.- Lift and moment characteristics of the model with tapered permeability from 0- to 1-percent chord and a 0.2-chord split flap deflected 60°; V_0 = 133 fps.

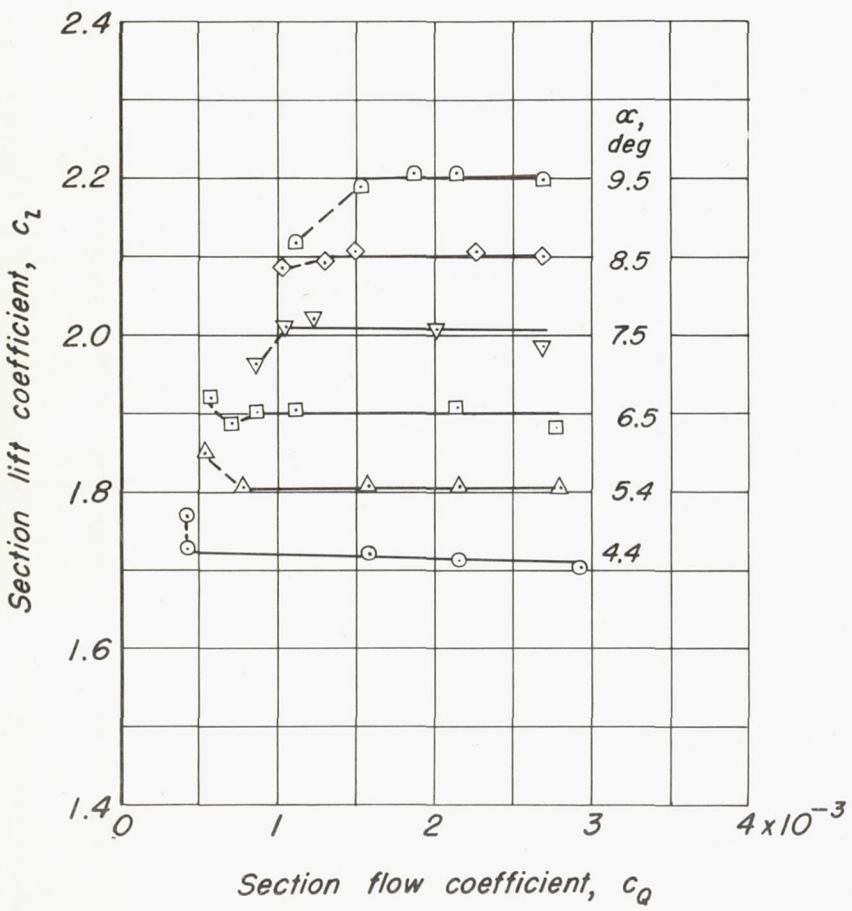

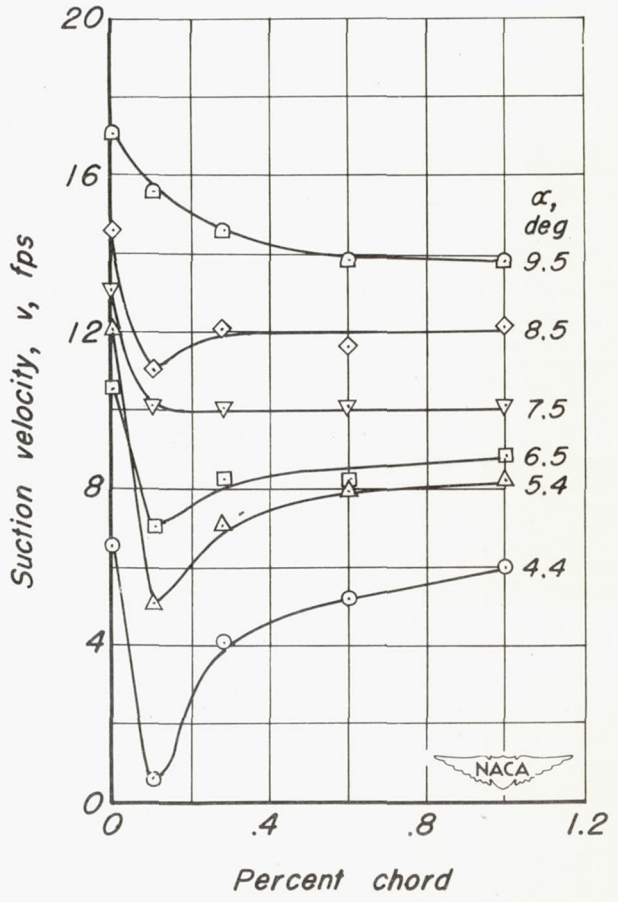

Figure 18.- Flow requirements and stall-point suction-velocity distributions for the model with tapered permeability from 0- to 1-percent chord and a 0.2-chord split flap deflected 60°; V_o = 133 fps.

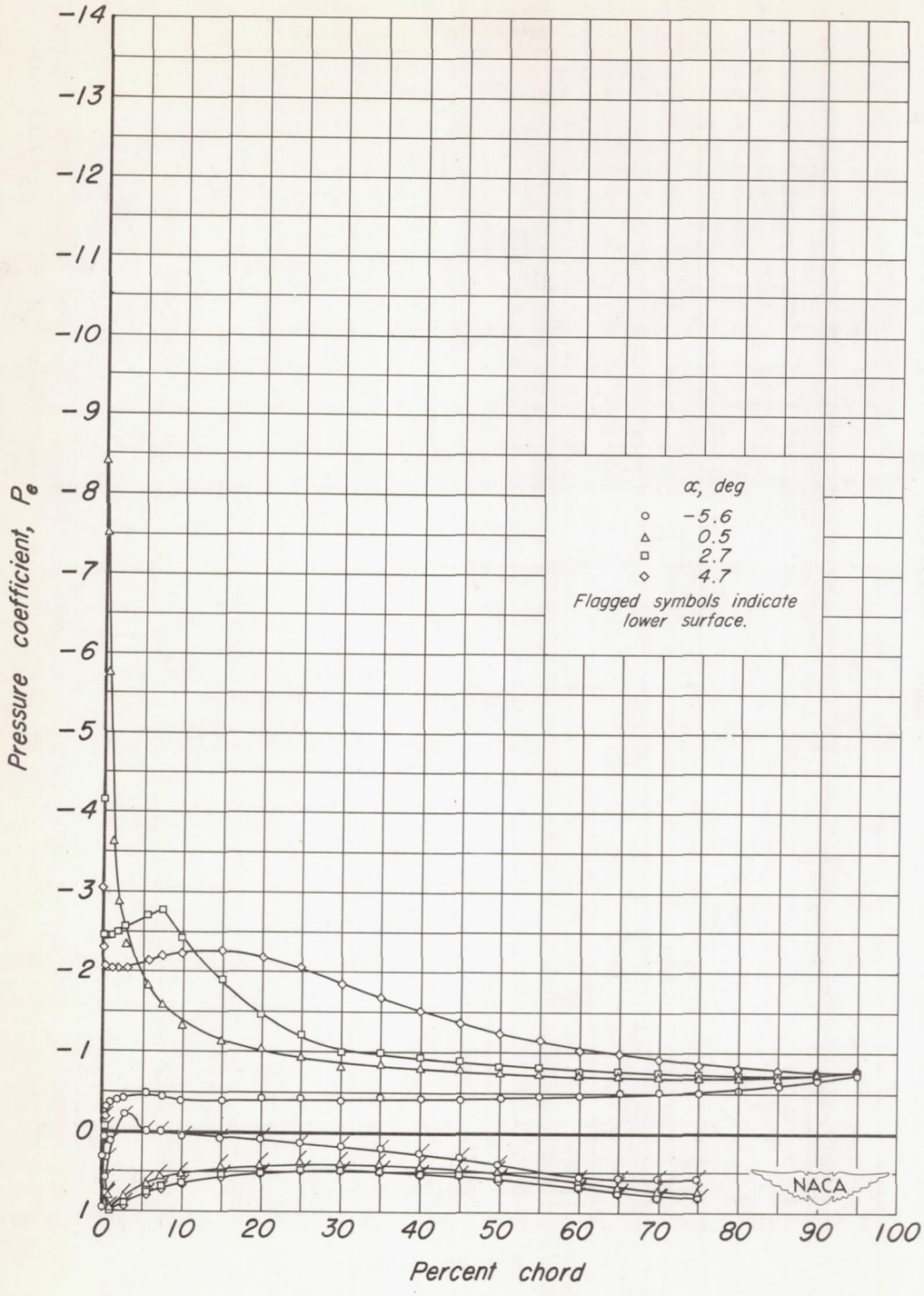

(a) Plain airfoil.

Figure 19.- Pressure distribution over the model with a 0.2-chord split flap deflected 60°; V_0 = 133 fps.

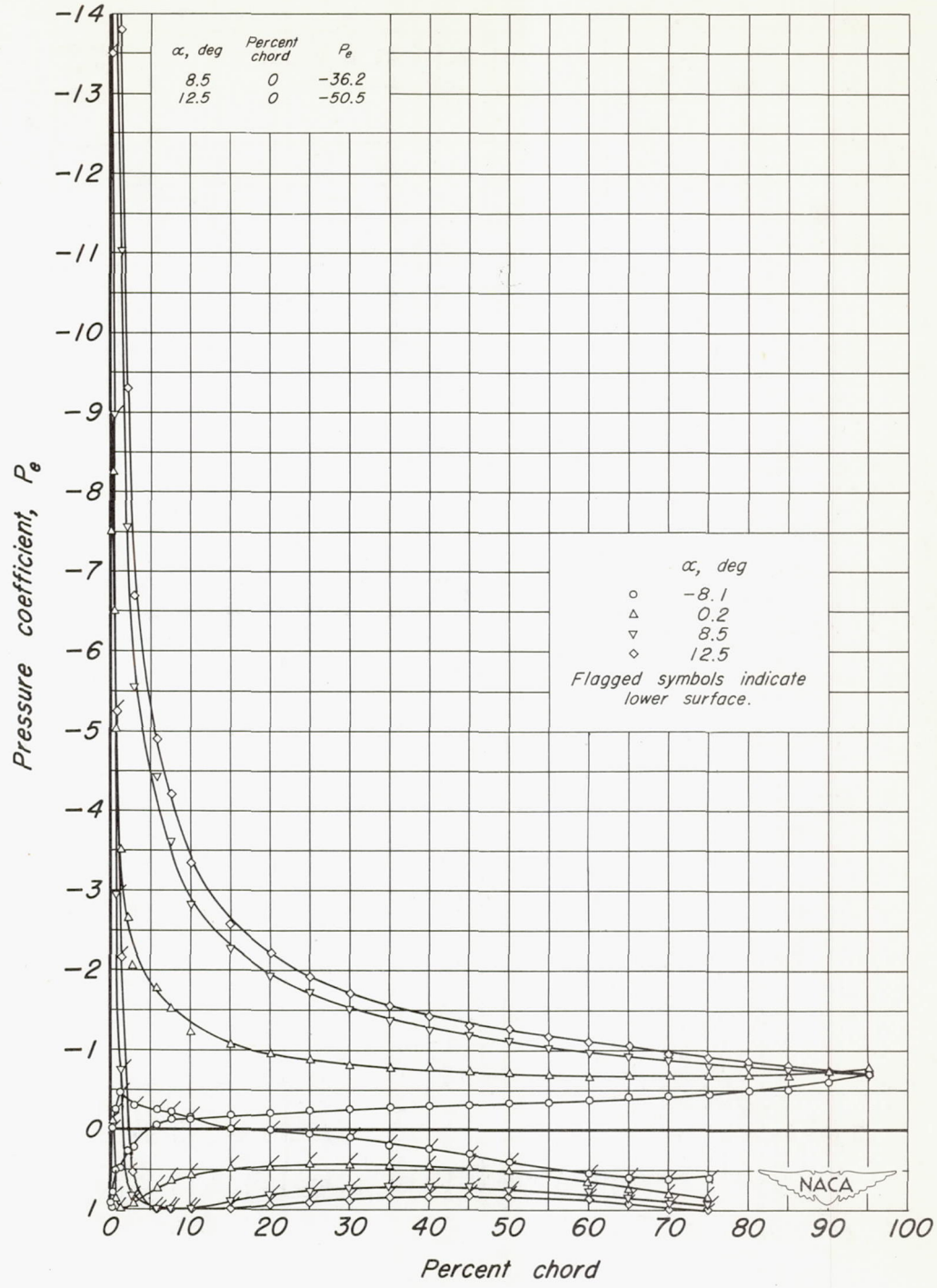

(b) Model with tapered permeability from 0- to 1-percent chord; $c_Q = 0.0027$.

Figure 19.- Concluded.

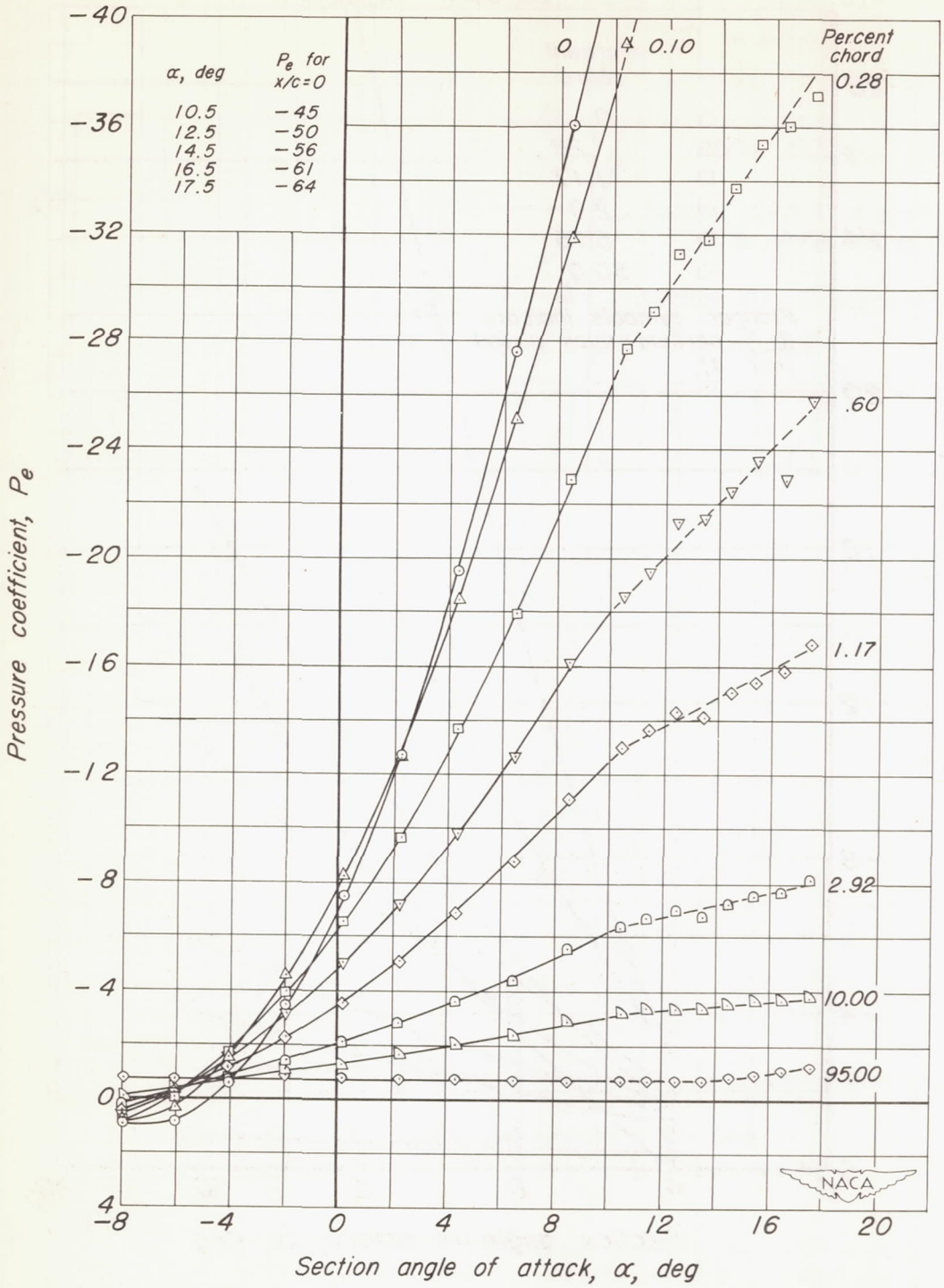

Figure 20.- Variation of the pressure coefficients at particular chordwise stations with angle of attack with a 0.2-chord split flap deflected 60°; tapered permeability from 0-to 1-percent chord; $c_Q = 0.0027$; $V_0 = 133$ fps.

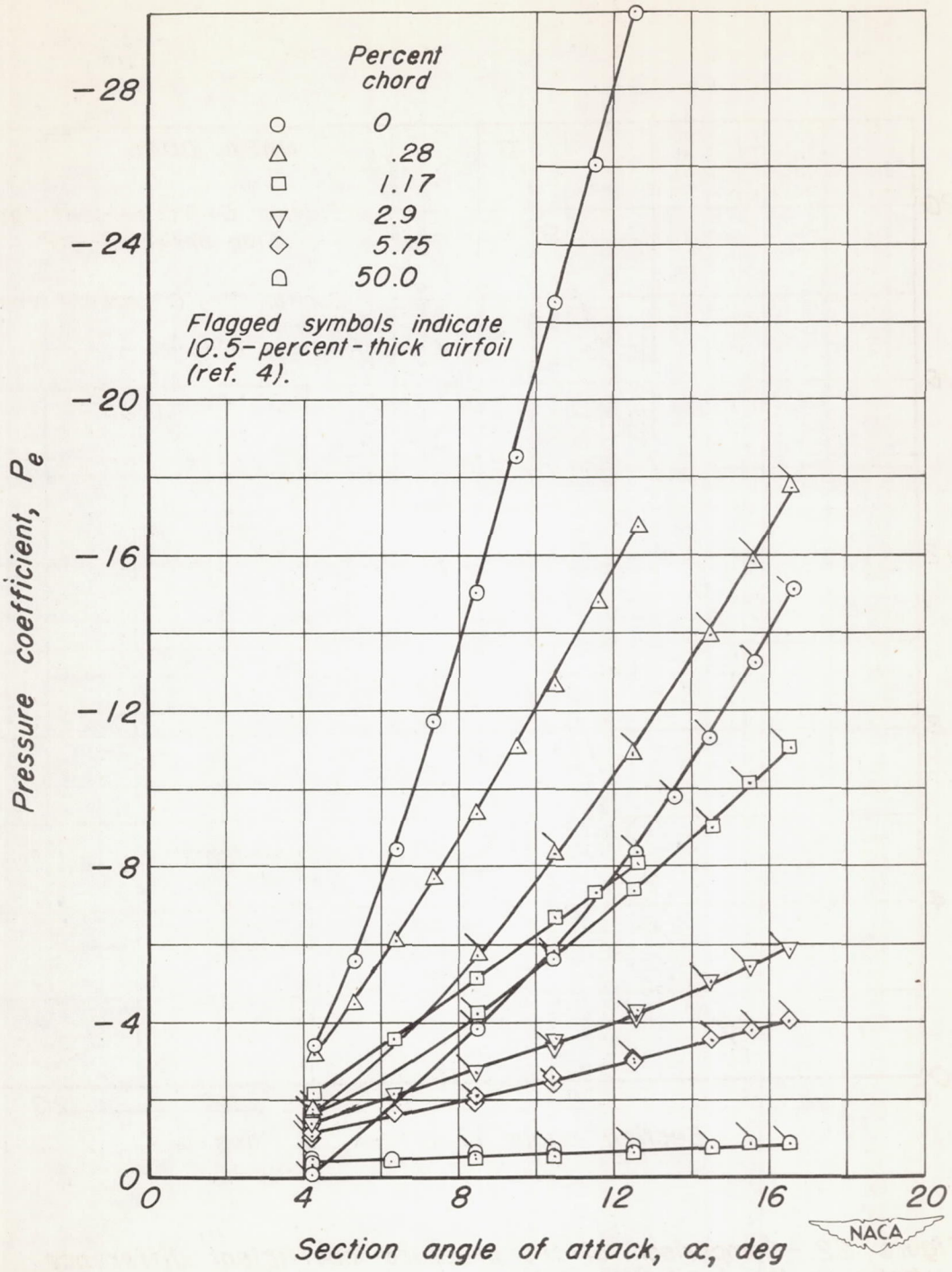

Figure 21.- Comparison of the pressure coefficients on the NACA 0006 and the symmetrical 10.5-percent-thick airfoils; c_Q = 0.0016; V_0 = 162 fps.

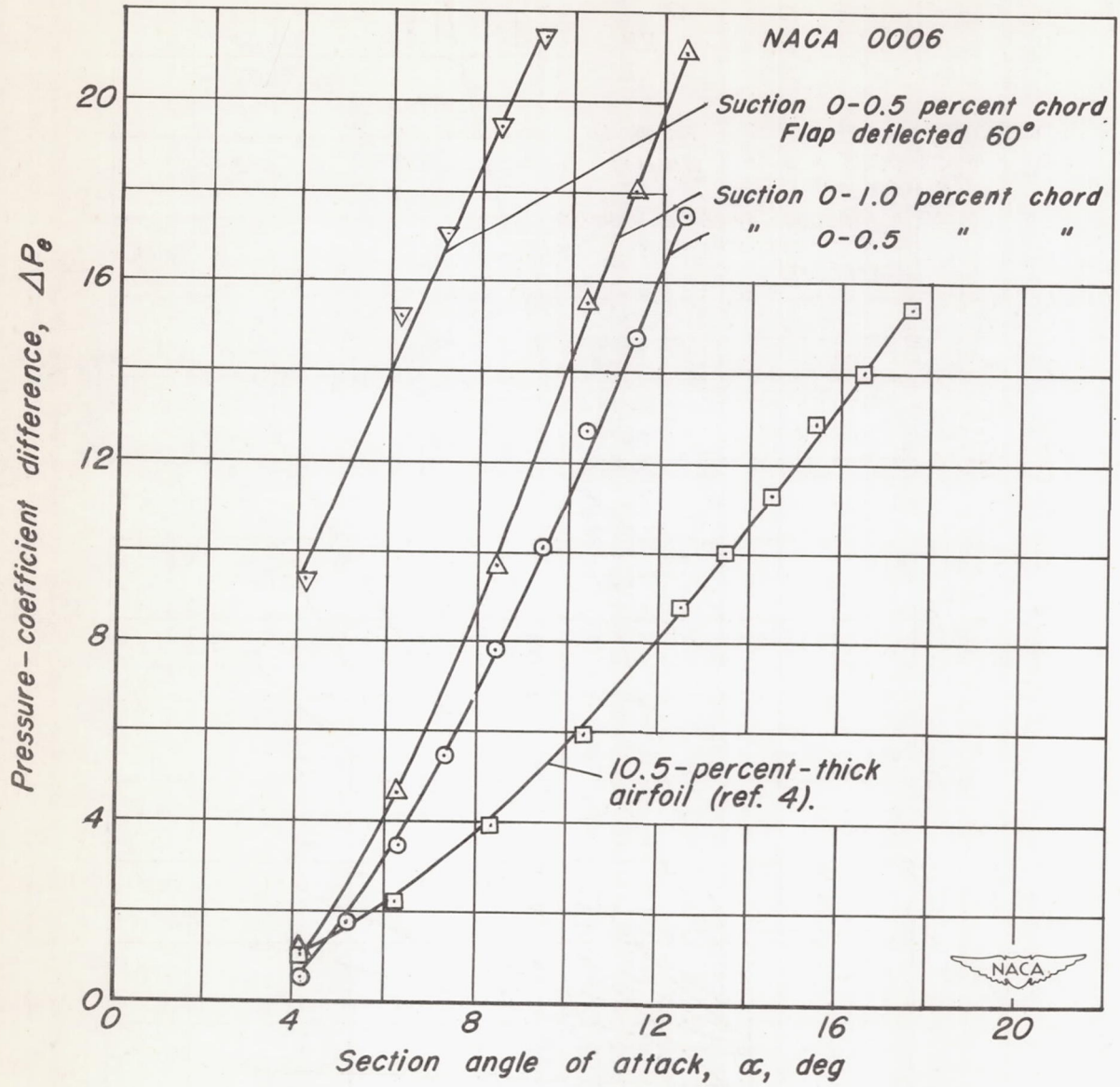

Figure 22.-Comparison of the pressure-coefficient difference between the leading and trailing edges of the porous area on the NACA 0006 and the symmetrical 10.5-percent-thick airfoils; $c_Q = 0.0016$; $V_0 = 162$ fps.

	Airfoil	Permeability	Extent of porous area, percent	V_o, fps
○	NACA 0006	Tapered	0 to 0.5	93
△	"	"	"	133
□	"	"	"	162
▽	"	"	"	187
◇	"	"	0 to 1.0	162
▱	10.5-percent-thick	K (ref. 4)	0.3 to 3.0	162
▷	NACA 0006 with 0.2 chord split flap at 60°	Tapered	0 to 0.5	162

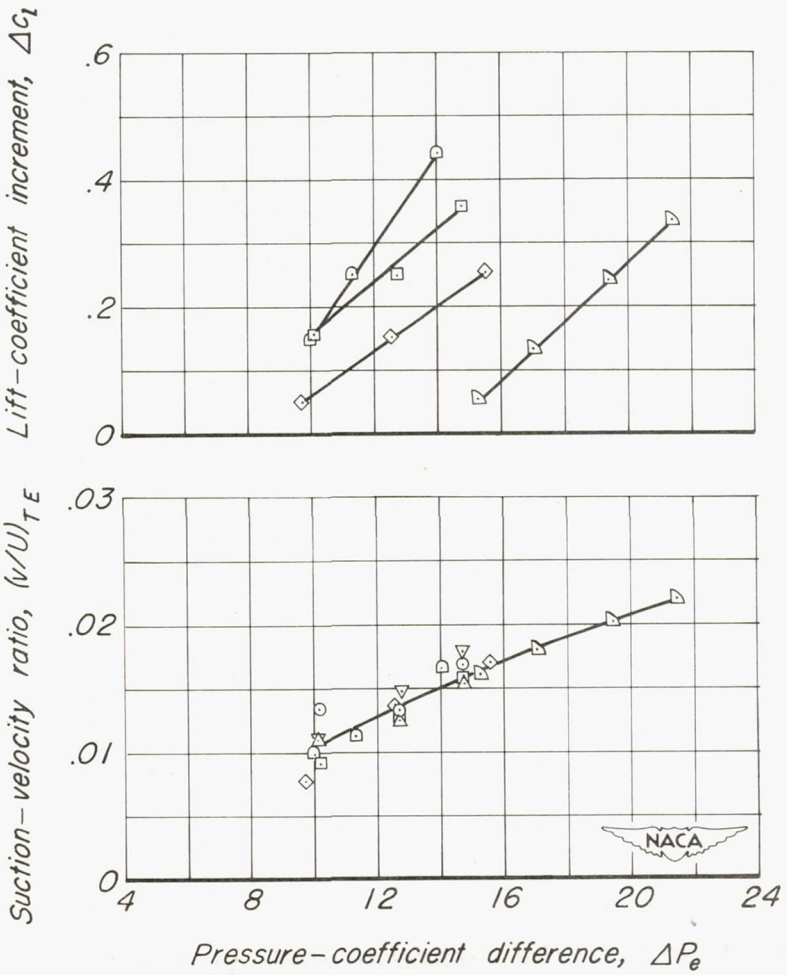

Figure 23.- Variation of the stall-point suction-velocity ratio and lift-coefficient increment with pressure-coefficient difference between the leading and trailing edges of the porous area.

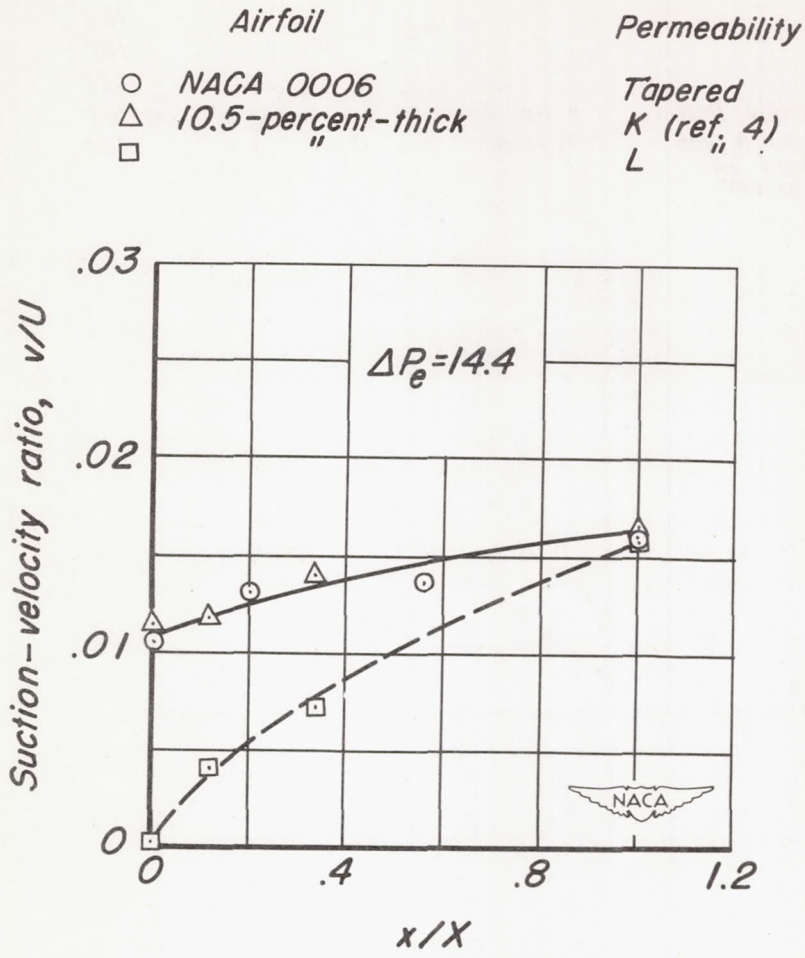

Figure 24.- Comparison of the stall-point suction-velocity distributions on the NACA 0006 and the symmetrical 10.5-percent-thick airfoils; V_0 = 162 fps.